DATE ISSUED MAY 1 1 1982

ORNL
MASTER COPY

ORNL/TM-7895

OAK RIDGE NATIONAL LABORATORY

UNION CARBIDE

Negative Ion Beam Generation with the ORNL SITEX Source

W. K. Dagenhart
W. L. Stirling
J. Kim

OPERATED BY
UNION CARBIDE CORPORATION
FOR THE UNITED STATES
DEPARTMENT OF ENERGY

Printed in the United States of America. Available from
National Technical Information Service
U.S. Department of Commerce
5285 Port Royal Road, Springfield, Virginia 22161
NTIS price codes—Printed Copy: A05; Microfiche: A01

[illegible]

ORNL/TM-7895
Dist. Category UC-20

Contract No. W-7405-eng-26

FUSION ENERGY DIVISION

NEGATIVE ION BEAM GENERATION WITH THE ORNL SITEX SOURCE

W. K. Dagenhart, W. L. Stirling, and J. Kim

Date Published - May 1982

NOTICE This document contains information of a preliminary nature. It is subject to revision or correction and therefore does not represent a final report.

Prepared by the
OAK RIDGE NATIONAL LABORATORY
Oak Ridge, Tennessee 37830
operated by
UNION CARBIDE CORPORATION
for the
DEPARTMENT OF ENERGY

CONTENTS

ABSTRACT v

INTRODUCTION 1

I. EXPERIMENTAL APPARATUS 5

A. Plasma generator 5

B. Cesium supply 7

C. Extraction and optics 14

D. Ion source assembly 14

E. Electron recovery system 21

F. Test facility 26

G. Instrumentation 28

II. EXPERIMENTAL RESULTS 31

A. H^- beam current and current density 31

B. H^- converter and converter materials 34

C. Gas efficiency 43

D. Electron control 45

E. Long pulse/dc operation 49

F. Optics 56

G. Impurities 56

III. DISCUSSION 67

A. Error analysis 67

B. Plasma generator 67

C. H^- loss mechanisms 69

D. Comparison of surface conversion negative ion sources 69

ACKNOWLEDGMENTS 71

REFERENCES 73

ABSTRACT

Parametric studies were made on a hot cathode reflex discharge H^- Surface Ionization source with Transverse Extraction (SITEX) in both the pure hydrogen and the mixed hydrogen-cesium mode. Extraction current density, beam current, gas efficiency, extracted electron-to-H^- current ratio, heavy negative ion impurities, optics, and long pulse operation were investigated as a function of time, arc voltage, arc current, converter voltage, H_2 gas flow, cesium feed rate, and plasma generator geometries. Initial results of the research were an extracted H^- beam current density of 56 mA/cm^2 at 23 mA for 5 s pulses and, gas efficiency of 3%, $\theta_\perp$ (1/e) $\sim 2 \pm 1°$, $\theta_\parallel$ (1/e) $\sim 1 \pm 1°$, at a beam energy of 25 keV. Negative heavy ion beam impurities were reduced to <1% at low current densities. H^- ions are produced principally by positive ion surface conversion using elemental cesium fractional monolayer coverage on a molybdenum converter substrate, which is biased negatively with respect to the anode.

INTRODUCTION

Recent tokamak plasma fusion devices such as the Princeton Large Torus[1] (PLT) and the Poloidal Diverter Experiment[2] (PDX) at the Princeton Plasma Physics Laboratory (PPPL) and the Oak Ridge Tokamak[3] (ORMAK) and the Impurity Study Experiment[4] (ISX-B) at the Oak Ridge National Laboratory (ORNL) have successfully used high power, positive-ion-based neutral beam heating of the plasma with systems developed at ORNL. Research on PLT has established record high plasma temperatures of $\sim$7.5 keV with $\sim$2.4 MW of injected D^0 power at 40 keV from four beam lines. This successful heating technique will also be used on the Tokamak Fusion Test Reactor[5] (TFTR), which is located at PPPL, at neutral beam energies of 120 keV. Calculations indicate that demonstration[6] and power reactor[7] tokamak bulk plasma heating by neutral beams may require beam energies in the range of 120-250 keV, with a total power from all beams of $\sim$70 MW for $\sim$10 s. Current drive, profile control, and impurity control scenarios may require energies hundreds of kiloelectronvolts above this. Mirror reactors,[8] which are being investigated at the Lawrence Livermore National Laboratory (LLNL), will place even more stringent requirements on neutral beam heating systems. For mirror reactors, the different neutral beam systems must operate at steady state and at beam energies up to 400 keV.

High energies above 100 keV per nucleon are clearly out of the practical range of positive-ion-based systems[9,10] due to a greatly reduced neutral equilibrium fraction at high energies, as shown in Fig. 1. For example, the neutral fraction produced by passing a (150/200)-keV D^+ beam through D_2 gas is (34/13)%.[11] When this neutralization efficiency is coupled with the best ORNL source optics of 0.5° (HWHM) at 70 keV demonstrated to date, which produced an 80% beam transmission[12,13] through a ±2° aperture, we get a neutral power-to-input power ratio of $\leqslant$(10/27)% for H^+/D^+ ions at 150 keV. With the energy recovery system recently developed at ORNL operating at 60% efficiency,[14-17] the beam system's power efficiency would be boosted to $\leqslant$(14/32)% for H^+/D^+ ions at 150 keV.

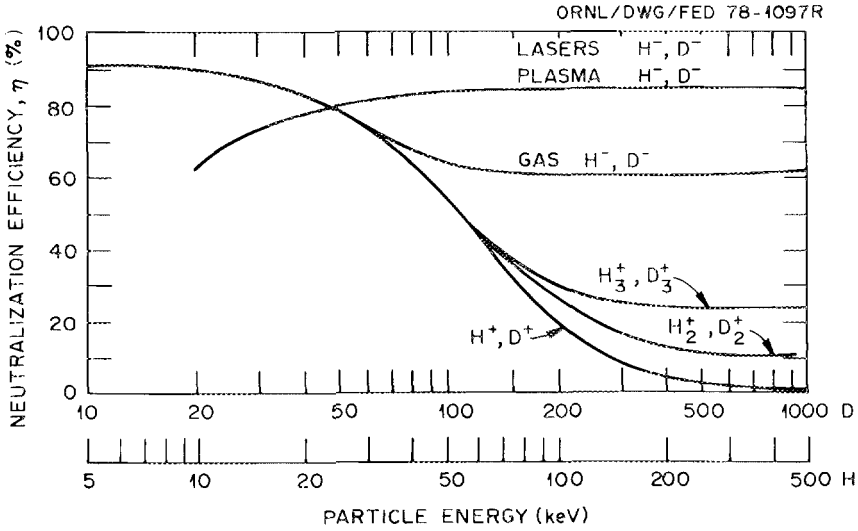

Fig. 1. Peak neutralization efficiency of different ion species as a function of ion energy (courtesy of K. Prelec).

High energy neutral beam heating systems based on negative ions offer a way of greatly increasing system efficiency. Several different H^-/D^- beam generation systems are currently under investigation for this purpose. High power negative ion beams have been produced at Lawrence Berkeley Laboratory (LBL)[18] and elsewhere by the double charge exchange method and at Brookhaven National Laboratory[19] (BNL) by surface ionization. At BNL D^- beams of 1 A at 130 keV at very short pulse lengths of 3 ms have been produced with a divergence of ±15°. Although these experiments were important in the development of negative ion beam systems, the ultimate suitability of the sources tested for reactor use is dependent on significant development in the areas of system design, gas efficiency, power efficiency, optics, and long pulse capability.

Initial results from 25-keV H^- beam extraction studies[20] at ORNL indicate that it may be possible to have negative ion beam optics as good as the present positive ion optics. With an early model advanced positive ion source, we have demonstrated that ∿80% of H^+ ions plus neutrals at ∿100 keV can be transmitted through a ±2° opening at 4 m from the source.[12,13] If the negative ion source achieves this quality optics, we could couple this with a D_2 gas neutralizer to produce a ≤53% power efficient beam line at 150 to >200 keV beam energy without energy recovery. An even more promising result can exist by using a laser-driven, photon-detachment neutralizer operating at a >90%[21] efficiency. A recent report at the BNL negative ion symposium indicated that a 1-MW laser system would be adequate for a 10-MW beam and could provide a >90%[22] neutral fraction. The net power efficiency from a laser-neutralized, negative-ion-based system could be as high as 75%; this efficiency should be achievable in the energy range of 100-∿600 keV, where multigap direct extraction is possible.[23,24] This efficiency could also be achieved with two stages of acceleration using present ion sources at the cost of more hardware complexity.

I. EXPERIMENTAL APPARATUS

The studies in this paper utilized both an existing Calutron test facility and ion source assembly that were both modified for the purpose of these experiments. Changes that were made include a new plasma generator, a cesium oven and valve control, a new electron control system, and new accelerator electrodes. In its original configuration,[25] this ion source produced over 0.5 A of Ca^+ ions at 35 keV. With an expanded plasma generator and multiple slits, this source assembly would be large enough to produce an ∿10-A, H^-/D^- beam at 40 kV. This assumes we can achieve 120 mA/cm^2 output at the emission slit.

A. Plasma generator

Figure 2 shows an elementary drawing of the plasma generator concepts used in the present experiments. A hot tantalum filament emits electrons that are drawn to the anode along magnetic field lines by ∿100-200 V(dc). H_2 gas admitted near the filament collides inelastically with the energetic electrons to form an intense arc discharge. Primary electrons with arc voltage energies stream through an anode collimating slot into a hollow anode chamber where they produce more hydrogen ions in addition to those produced in the filament region. These primary electrons, reduced in energy by inelastic collisions, stream through another collimating slot in the opposite side of the anode chamber and are reflected from a floating electrode that is self-biased by electron and ion currents. These electrons again enter the hollow anode chamber for further ionization collisions and oscillate in the chamber until they are thermalized or lost to the anode wall. The floating, reflecting electrode potential has been measured in other experiments and normally floats at 1 to 1-1/2 times the cathode voltage. If H_2 gas is admitted into the hollow anode chamber rather than into the cathode region, then twice as much gas is required to maintain the same discharge current and H^- beam current for a 2.54 cm long slit. Longer slits require a feed at both amode and cathode locations for optimum gas efficiency. A flat

ORNL-DWG 79-2264CR FED

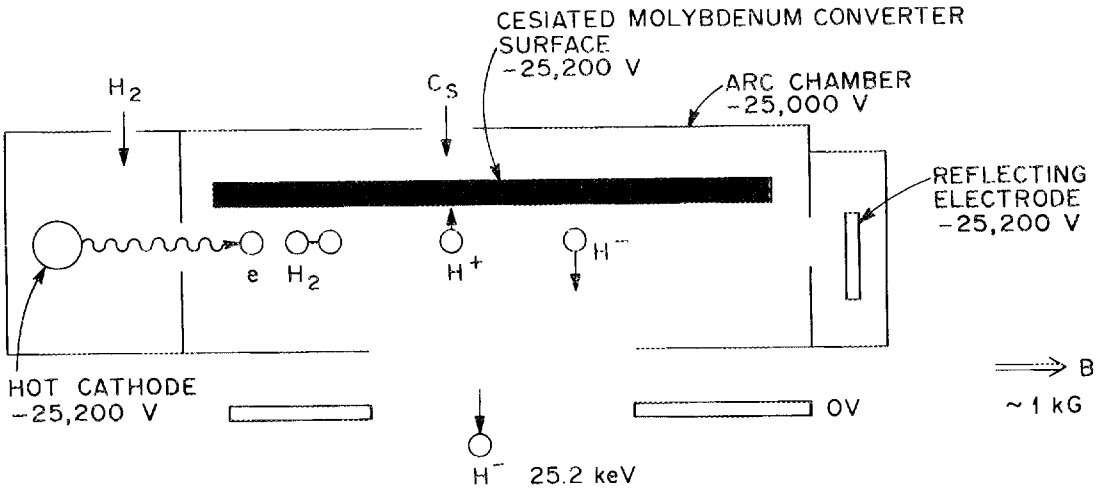

Fig. 2. Schematic diagram of a SITEX reflex arc discharge.

molybdenum converter electrode is placed directly behind the arc discharge and is connected to a bias supply, which can vary the converter potential from 0 to -250 V(dc) with respect to the anode. Cesium is admitted to the back of the arc chamber in order to provide a molybdenum converter coverage ∿3/4 of a monolayer, which has been reported to maximize the H^- yield from the surface.[26] Figure 3 shows a more detailed top view of this plasma generator with power supply connections except for that necessary to dispose of extracted electrons. In order to expedite these experiments, the arc chamber was constructed from an existing graphite assembly modified for this work. Until a suitable, actively cooled metal source is developed, graphite has made long pulse work possible without danger of destroying the source. Some parts did get hot enough with dc operation to sublime some graphite away from arc areas. Molybdenum was plasma sprayed on all graphite surfaces to a 0.05-0.1-mm thickness to prevent a cesium attack of the graphite and to minimize beam impurities.

Figure 4 shows a view of the filament/plasma generation area with the plasma grid removed. This grid seals the assembly so that gas admitted to the cathode area can only escape through the extraction slit. The tantalum plate to the left of the filament is maintained at filament potential so that the arc strikes only to the hollow anode or collimating slot. In this illustration gas is admitted to the middle of the anode canal which is 0.32 cm wide by 1.27 cm high by 1.9 cm long; more recent experiments admit the gas at the cathode end of this canal and result in slightly higher gas efficiency. Boron nitride and ceramic insulators are used for gas seals and converter plate insulation. The floating electron reflector is mounted on ceramic insulators.

B. Cesium supply

The first experiments completed had elemental cesium generated from the reaction $2Cs_2Cr_2O_7 + T_i \rightarrow 4Cs + Ti(Cr_2O_7)_2$.[27] Titanium powder and cesium dichromate were added stoichiometrically to an unsealed type 304L stainless steel container enclosed by a graphite heater oven assembly shown in Figs. 5 and 6. Pure sand was added to the mixture (25% by

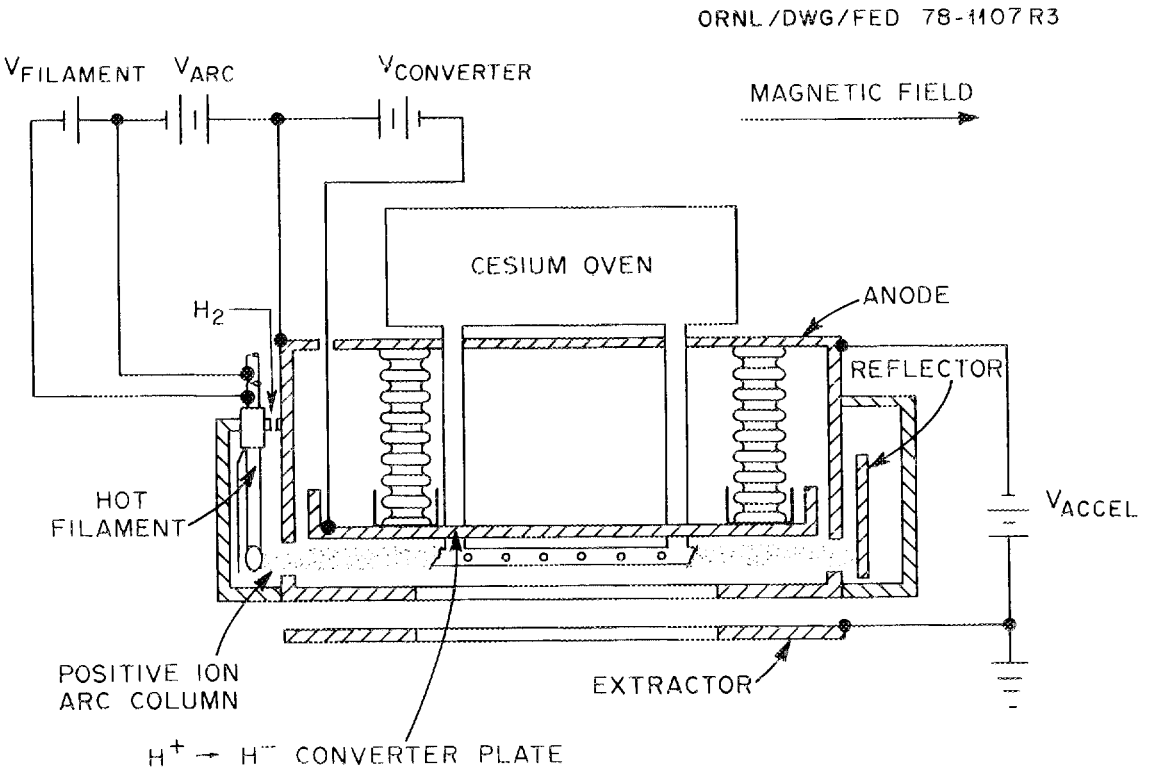

Fig. 3. Cross section of the plasma generator.

ORNL-PHOTO 4290-81

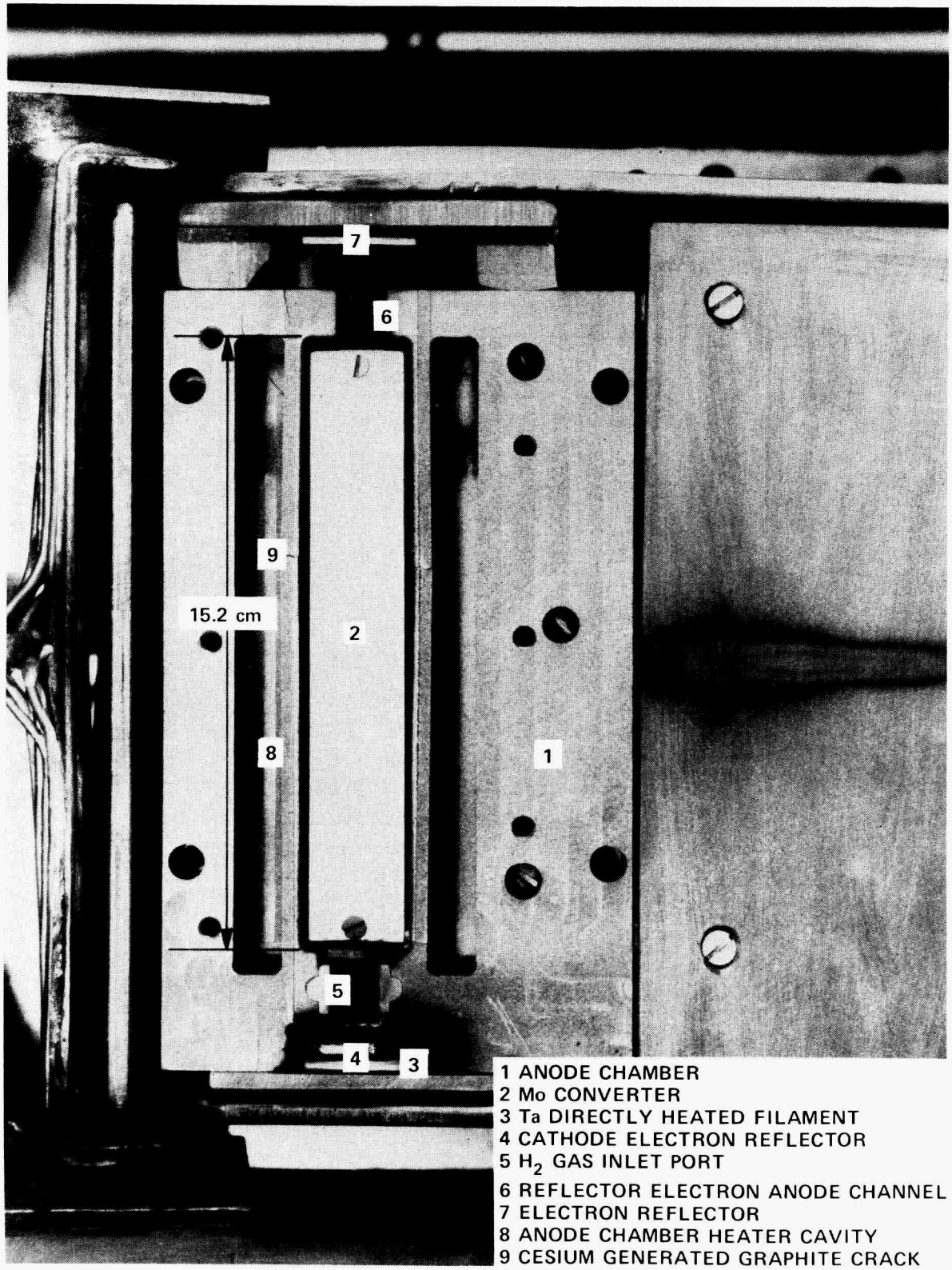

Fig. 4. Front view of the partially disassembled plasma generator.

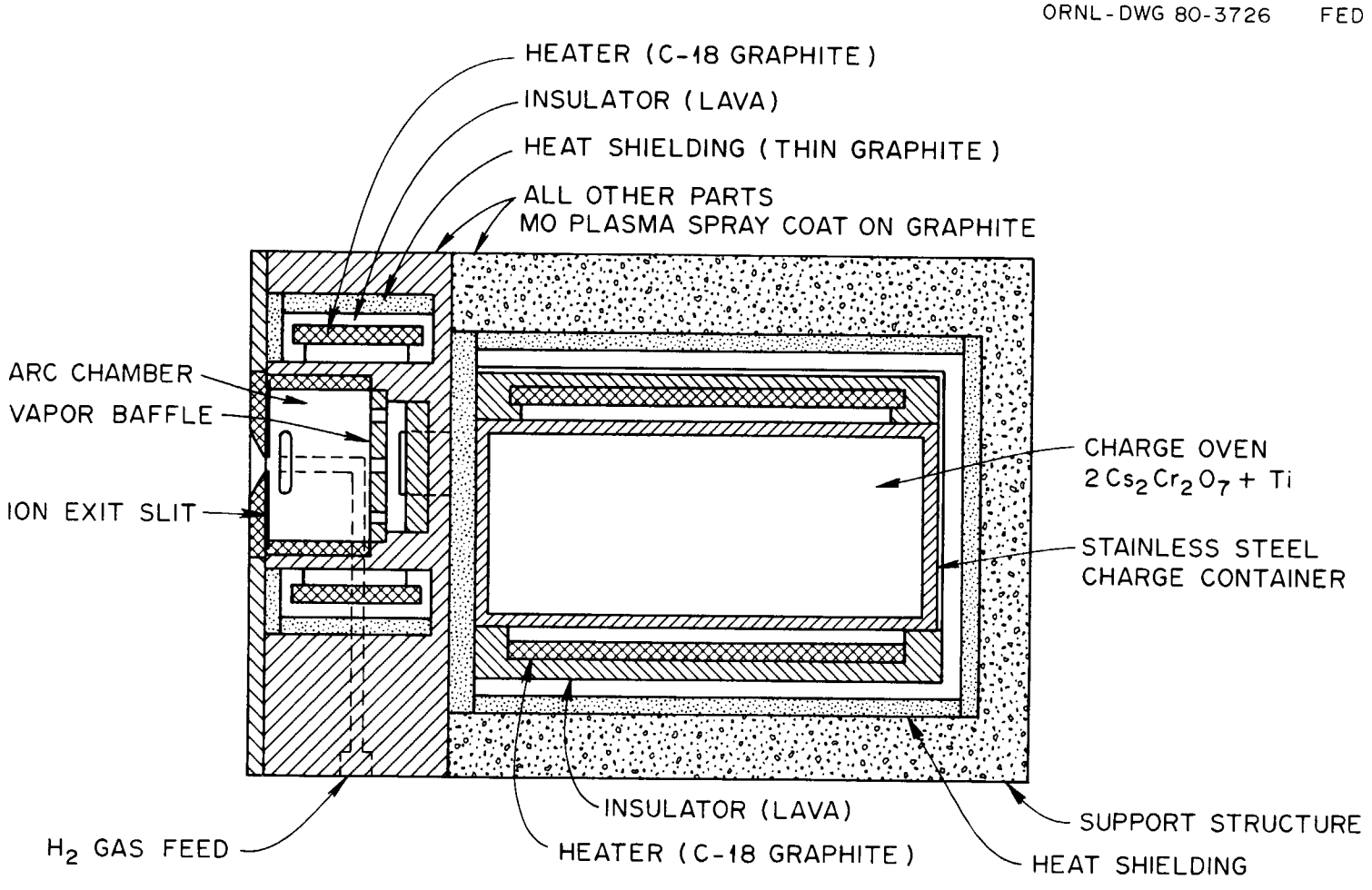

Fig. 5. Cesium dichromate oven assembly cross section.

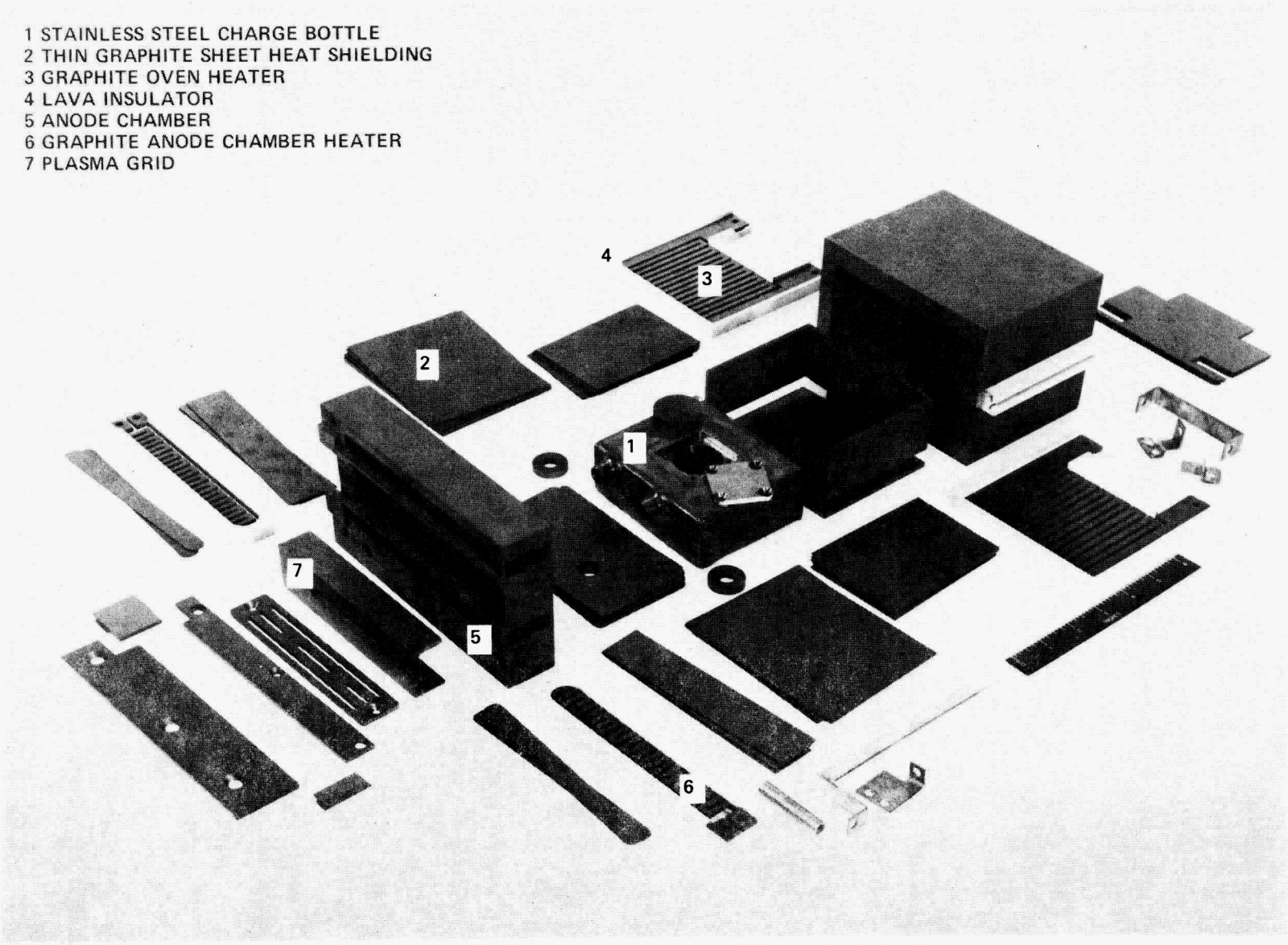

Fig. 6. Cesium dichromate oven assembly exploded view.

weight) to help control the exothermic reaction. This reaction has been used successfully by others[28-30] to produce cesium-coated surfaces for generating negative ion beams. The oven heater was a 0- to 1.5-kW unit machined from a graphite sheet. A 0- to 1.5-kW unit resistance heater was also installed around the arc chamber for degassing and cesium vapor deposition control. Figure 7 shows the oven plasma generator and degas heater pictorially. Cesium entered the plasma generator anode cavity through two 2.5-cm-long by 0.3-cm-diam stainless steel tubes directly behind the converter. To be useful the cesium eventually had to be transported to the front converter surface. One experiment was performed with the cesium manifolded to the front area of the anode cavity, where it diffused out of orifices directly aimed at the converter front surface. All data reported on here were gathered with the first configuration.

Due to excessive, heavy mass negative ion beam impurities >10% (see section II G) the cesium dichromate method of cesium production was replaced by one using elemental cesium metal in a temperature-controlled oven. In this mode of operation, the type 304L stainless steel cesium bottle is sealed and has a metal valve with a high temperature capability (723 K) to control the outlet conductance. The cesium bottle is again heated by a resistance heater; the bottle temperature transducer is a platinum resistance element. An isolation transformer reflects the resistance into a ground ac bridge, which generates a signal for automatic temperature control via the resistance heater. A manually actuated 60 rps motor is used to regulate the cesium valve. Cesium injection is again in the back of the anode chamber, but in future models will be directly on the front of the converter. The type 304L stainless steel transport tube from the oven to the anode chamber is kept hot by conduction from the arc chamber. To get smooth control, condensation must be prevented in the cesium transfer line. To accomplish this the anode chamber must be the hottest region with temperature monotonically decreasing back to the cesium bottle.

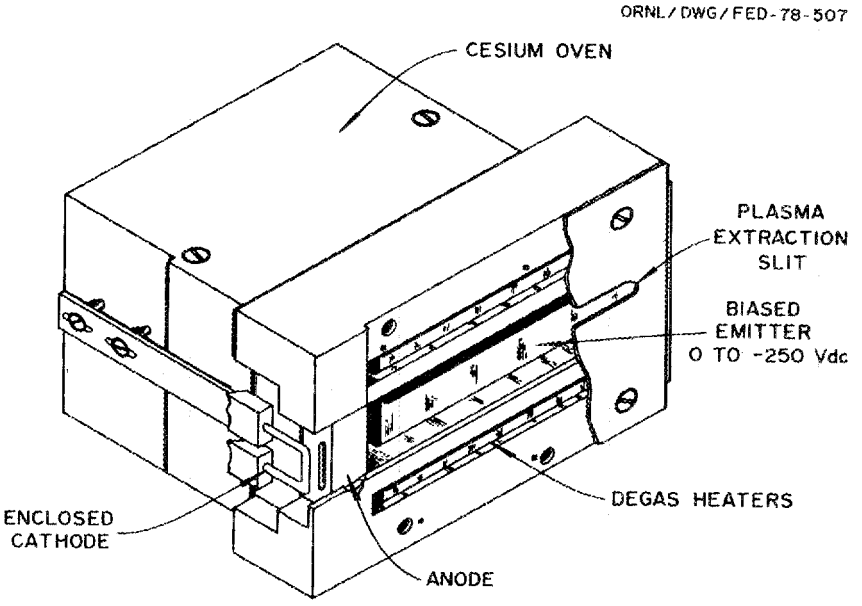

Fig. 7. SITEX oven-plasma-generator assembly.

C. Extraction and optics

Figures 8 and 9 show the geometry of the plasma generator electrode configuration used on most of these experiments. Because most of our initial trouble for several second pulses was in electron control and converter cesium control, not much effort was put into optics. Figure 9 shows a vertical cross section of the extraction optics and the 30° slit end correction in the plasma grid at the beam edge that had previously been used successfully on the 180° Oak Ridge Sector Isotope Separator.[31] The plasma grid extraction geometry represents easily machined dimensions, which have been used successfully before. Figure 10(a,b) shows a more recent extraction geometry in a progression toward higher gap fields. In this progression the gap has been reduced from 1.59 to 0.95 cm and run at the same extraction voltages. Gas efficiency and, hence, gap pressure and cesium presence will probably limit the acceleration field to less than those possible with H^+/D^+ ion sources. The structures for this study have been mostly uncooled molybdenum-coated graphite with occasional molybdenum or tantalum plates attached.

D. Ion source assembly

Figure 11 shows the modified Calutron ion source and attached diagnostic frame used for the present studies. Essentially the whole plasma generator, electron control, and extraction systems have been changed from the geometry used for isotope separation as a positive ion source. This ion source assembly is large enough to support a 1-A single or multiple slit H^-/D^- beam module or a 10-A multislit H^-/D^- beam module at 40 keV. A shielded calorimetric Faraday cup is shown on the front of the source for collecting the H^-/D^- beam after 90° of deflection in the homogeneous magnetic field in which it is immersed. Electrical, water, and mechanical motion services are fed through the high voltage insulators shown in the Fig. 12 cross-section of this source.

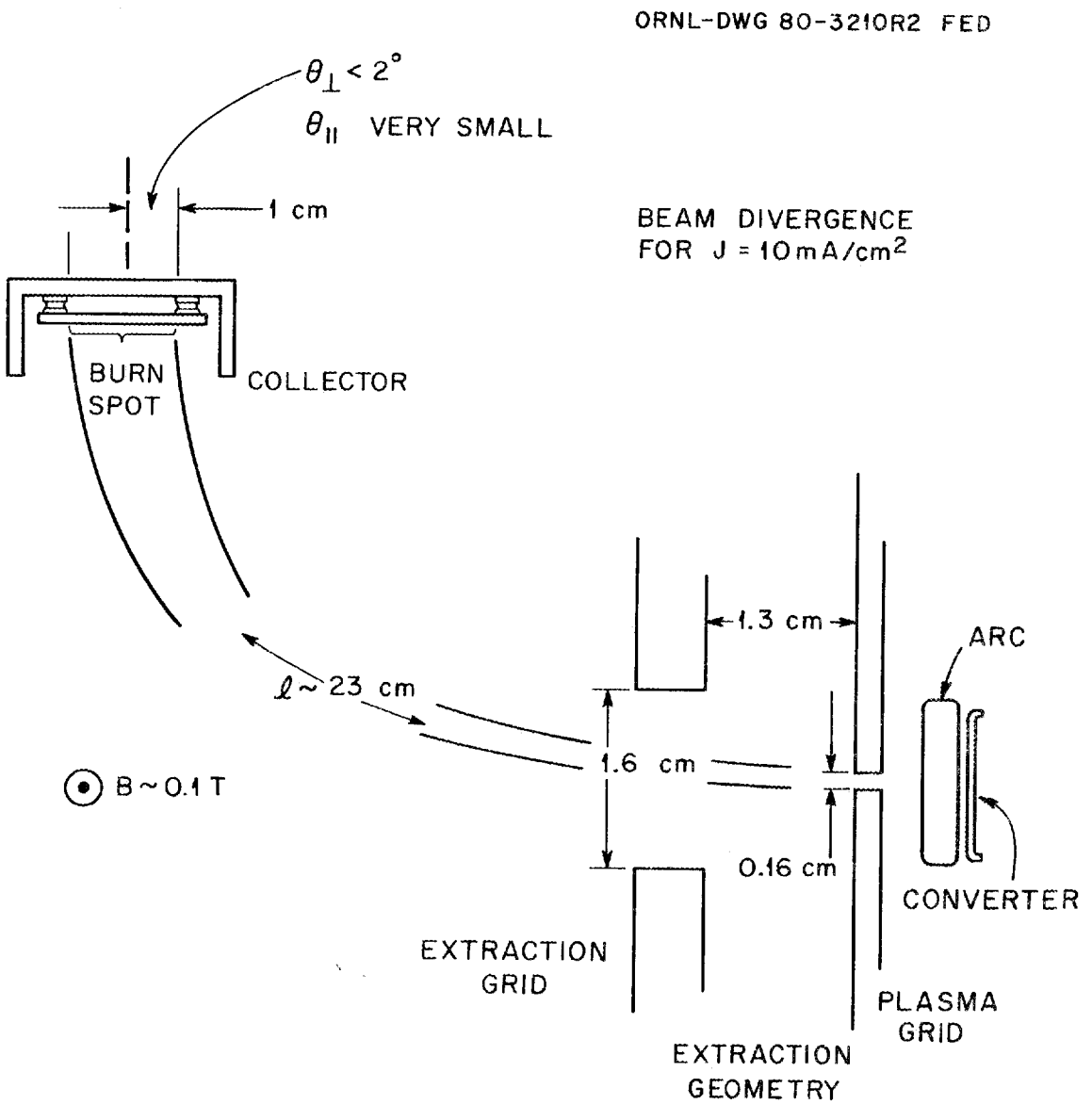

Fig. 8. Cross section of the first plasma generator and extraction optics in a plane perpendicular to the extraction slit.

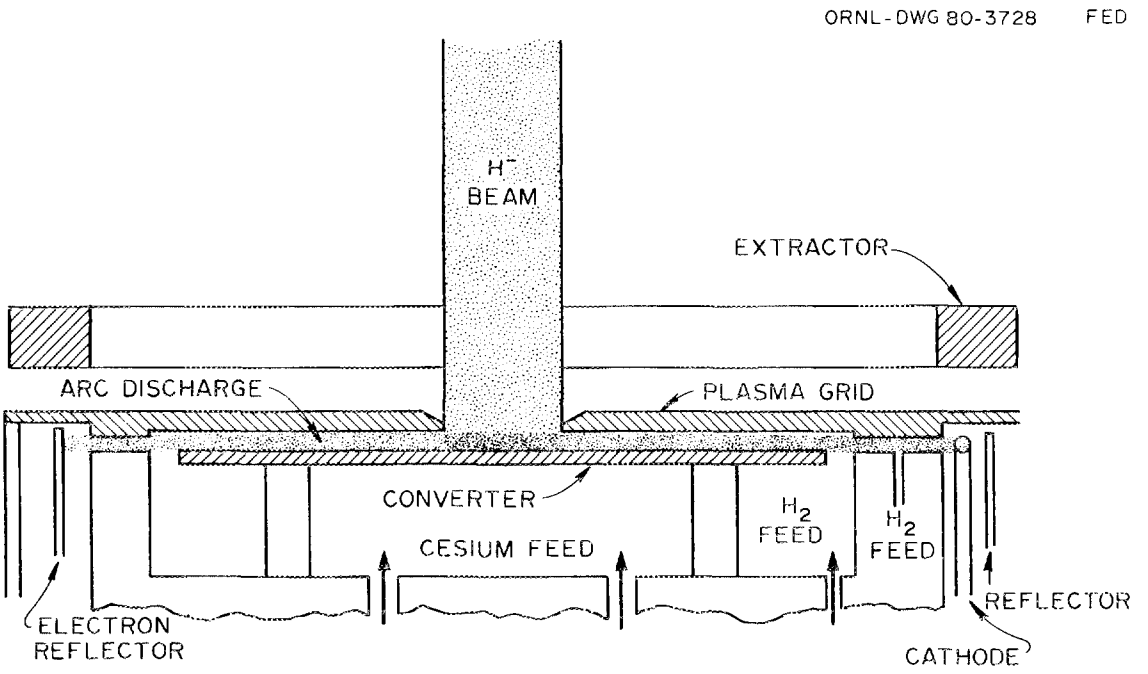

Fig. 9. Cross section of the first plasma generator and extraction optics in a plane perpendicular to the converter and containing the extraction slit.

ORNL-DWG 80-3729R FED

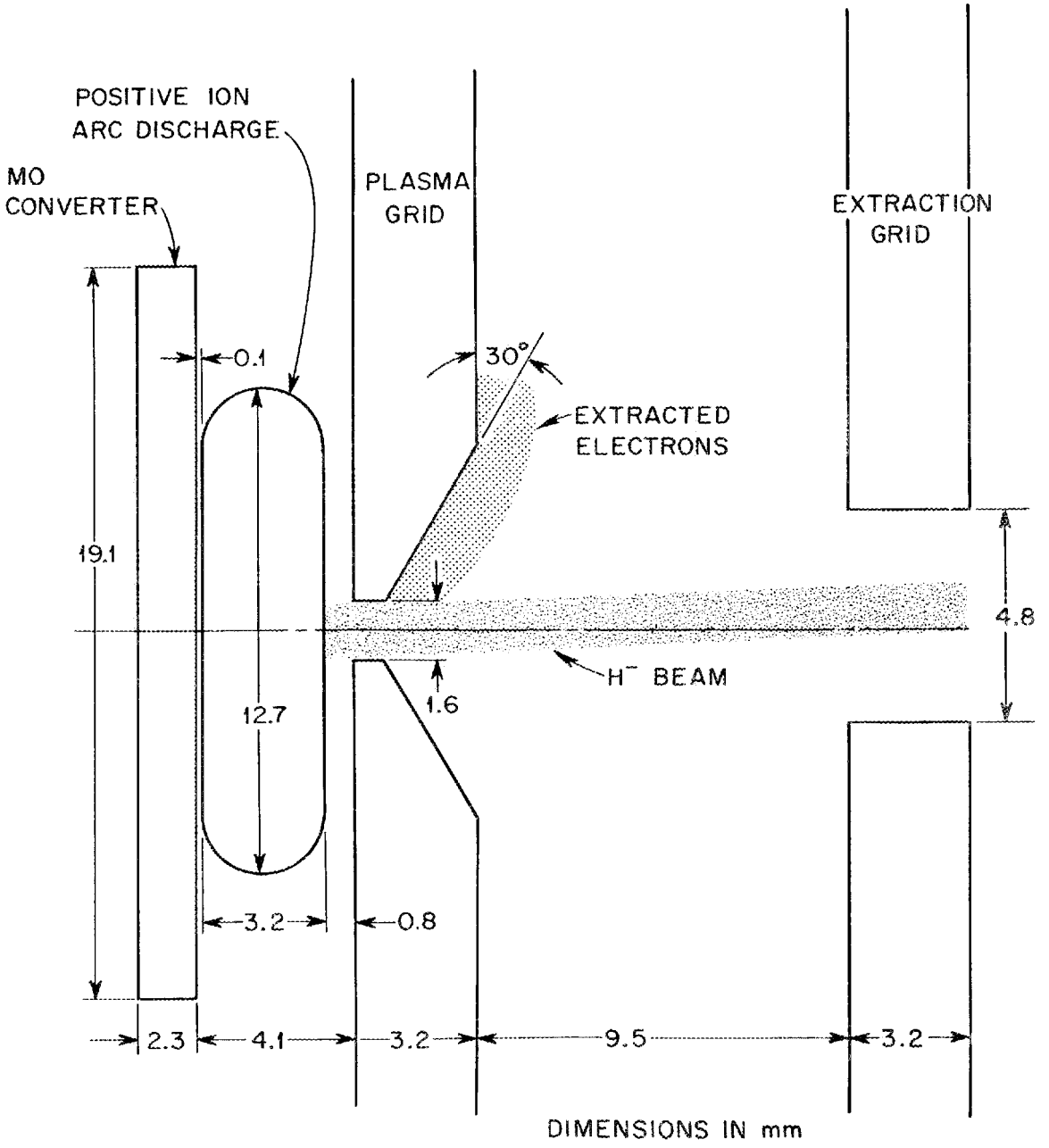

Fig. 10(a). Most recent extraction geometry cross section perpendicular to the plasma grid slit.

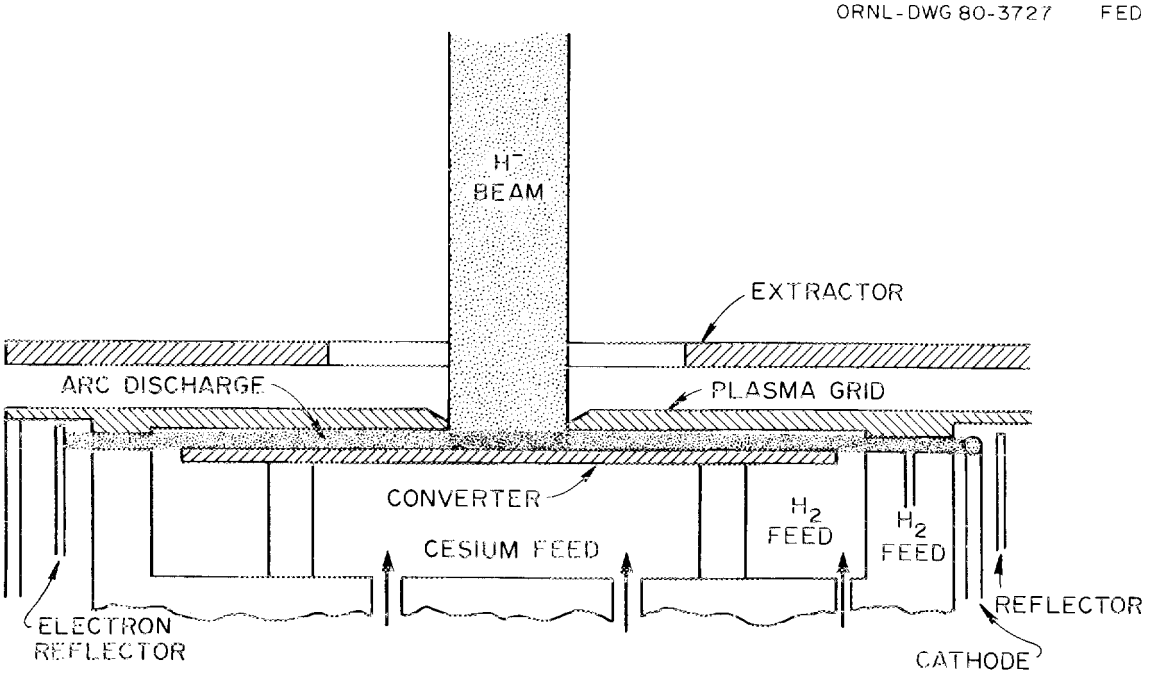

Fig. 10(b). Most recent extraction geometry cross section parallel to the plasma grid slit.

ORNL-PHOTO 7090-78

Fig. 11. SITEX ion source for H^-/D^- beam production.

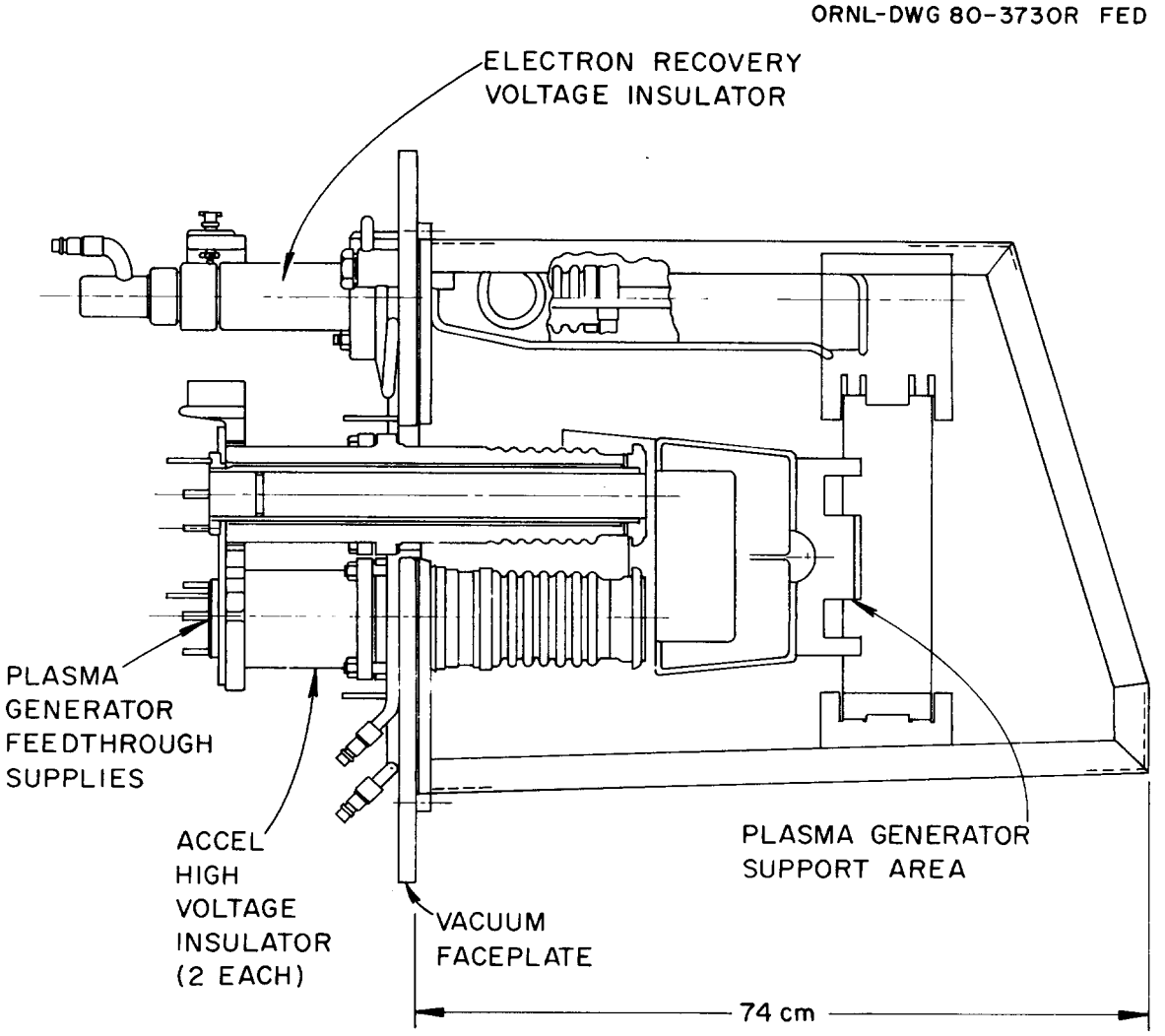

Fig. 12. Cross section of the SITEX source ion for H^-/D^- beam production.

E. Electron recovery system

Even limited operation of the negative ion SITEX source with the original electron control system for positive ion beams[32] was impossible, due to many areas on the source where electrons were trapped on magnetic field lines in positive potential wells. These electrons generated more electrons by ionization of background gas; the electron current quickly exceeded the accelerating supply current capability and also caused local melting of components. These oscillating electron regions were eliminated by geometry changes and stable high voltage operation was then possible.

There was still a serious problem with electrons extracted with the H^- beam dumping to ground along the magnetic field in concentrated areas near the accelerating structure. For long pulse and dc operation, holes were melted in water cooled type 304L stainless steel jackets and inertial water cooled copper parts. Shown in Fig. 13 is a water cooled source ground electrode melt-down. The electron stream continued on to melt a 2.3-mm thick type 304L stainless steel water cooled jacket. Because one of the main goals was dc operation, emphasis was placed on first reducing the electron energy loss. Because we have successfully lowered the electron power loss[33] (see section II D), arc operation is no longer restricted. We can freely examine arc geometries which might be more efficient for H^- generation but would produce larger I_e/I_{H^-} ratios without danger of melting the source or beam line components or incurring significant energy inefficiencies.

Figure 14 is an illustration of the electron recovery system showing the accelerating electrode, plasma grid extraction slit, electron recovery electrode, electron stream, impurity ions, and the H^-/D^- ion beam. Figure 15 shows the region between the electron recovery electrode and the anode chamber where a shaped region is introduced to provide an electric field component parallel to the magnetic field to dump the electrons on the electron recovery electrode. The electron recovery electrode is covered with a tantalum sheet screwed to a water cooled, copper structure shown in Fig. 16. As a result of this arrangement working the first time, no further developments have been made, and this

ORNL-PHOTO 4292-81

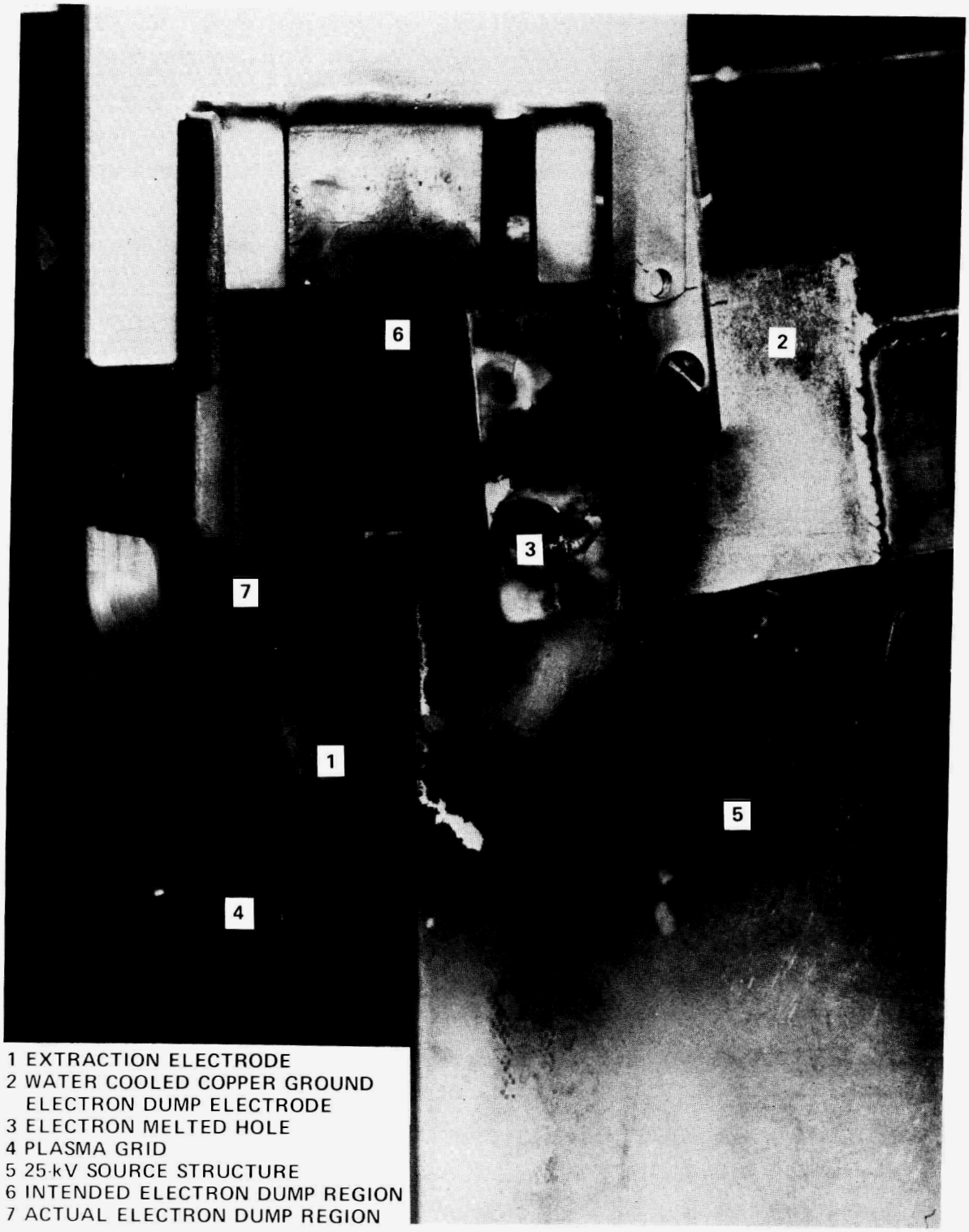

Fig. 13. SITEX ion source showing a hole melted in a water cooled copper ground plate by extracted electrons separated from the beam and collected at full 23-keV extraction energy for dc operation.

ORNL/DWG/FED 78-1072R

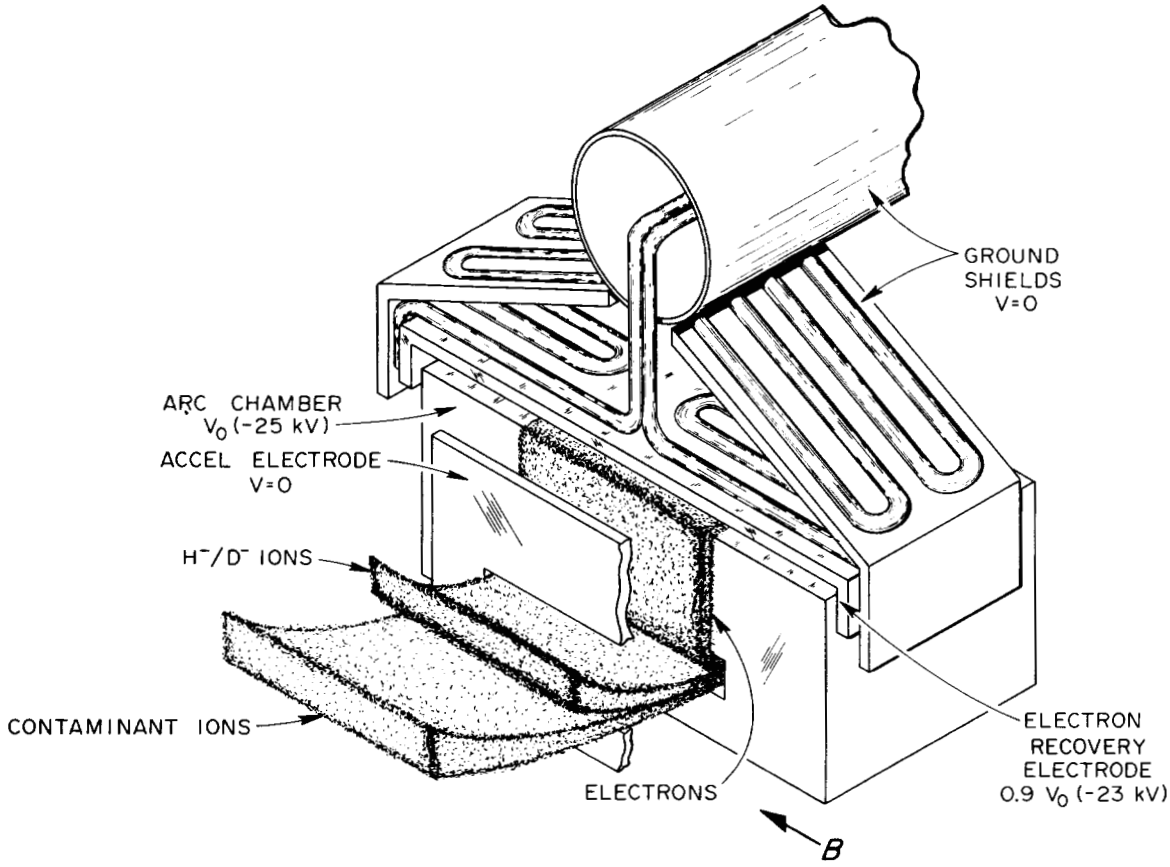

Fig. 14. Illustration of the electron recovery system.

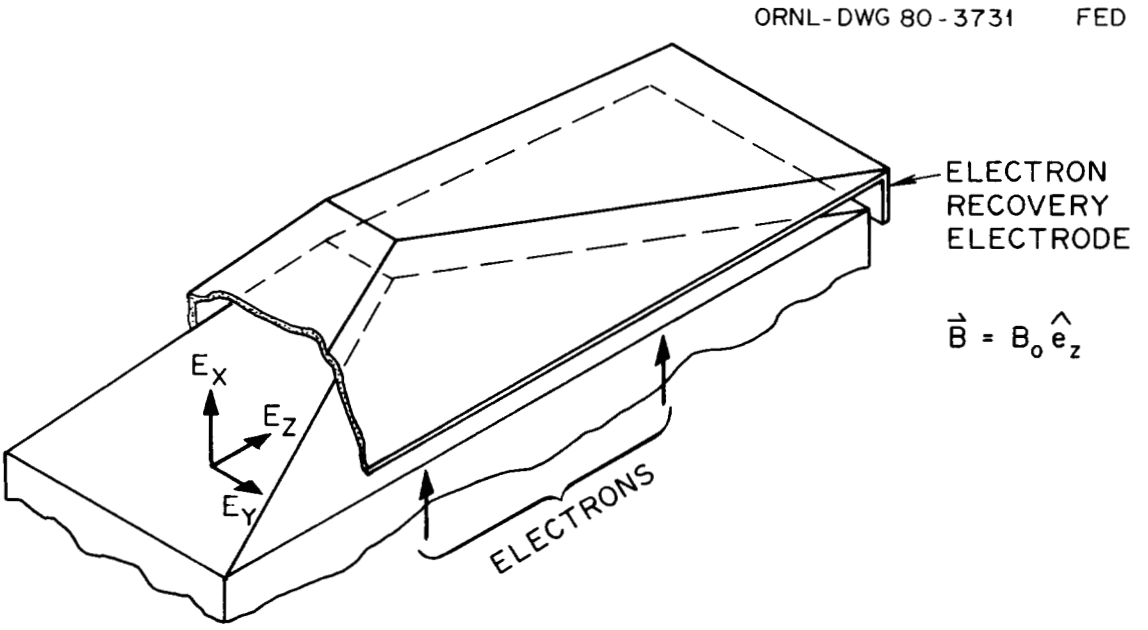

Fig. 15. Geometry of the electron recovery dump region.

ORNL-PHOTO 7155-81

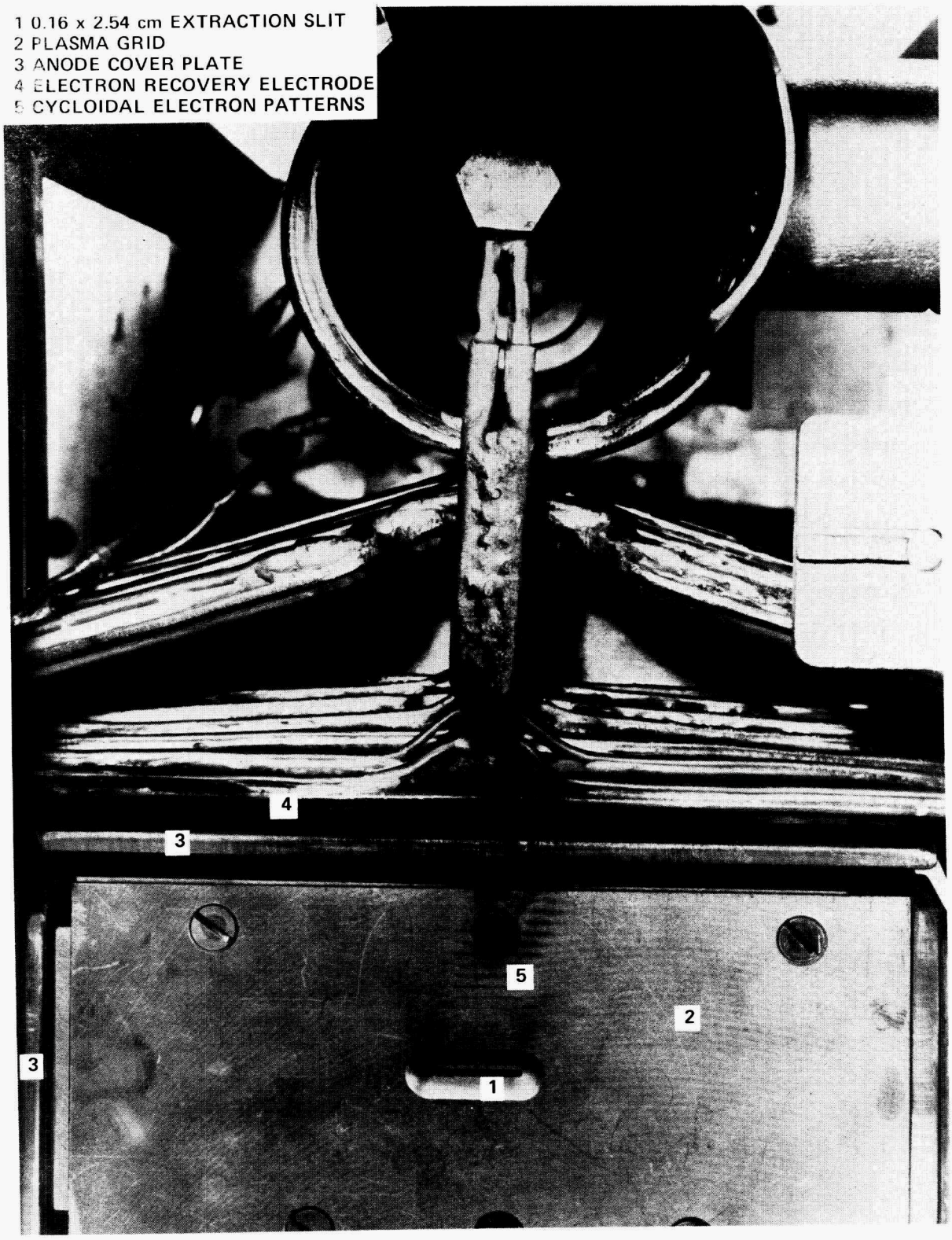

Fig. 16. Electron recovery electrode area.

structure should be sufficient for a H^-/D^- beam operation of >1 A without further development.

F. Test facility

All results contained in this study were obtained in a negative ion test facility composed of a modified beta Calutron isotope separator[34] and associated power supplies to which extensive diagnostics have been added. Figure 17 shows a section of a beta Calutron isotope separator vacuum tank and the placement of modifications. Vacuum was provided by two 20-in. oil diffusion pumps with manually operated gate valves. Pump heaters were modified to permit operation with Santovac-5 low vapor pressure organic diffusion pump oil. Previous work with a high resolution isotope separator encountered difficulty with insulating deposits from silicon-based diffusion pump oil. A freon refrigerated baffle at 233 K was mounted over the original jet assembly to further reduce oil backstreaming. Rough-down and fore vacuum were provided by 15- and 5-hp oil lubricated Kinney pumps, respectively, from the original 1940 facility.

The source, receiver, and all ion and electron beams are in an adjustable homogeneous magnetic field, which is usually 0.1 T. This dc field is provided by two large coils immediately adjacent to the vacuum tank and can be adjusted from 0-0.6 T. The heavy, negative ion mass spectrum, see section II G, is obtained by sweeping the negative ion beam over a slit apertured Faraday cup at the receiver, which is accomplished by modulating the coil current provided by a large motor generator. In normal operation, with H^- ions collected after 90° of deflection in front of the source on a 15-cm radius, we would have mass 16 monitored at $\Phi = 180°$ on a 60-cm radius. In addition, the heavy mass slotted aperture plate is long enough to monitor simultaneously a mass range of 13.7-18.6 amu. A wider mass range was investigated by varying the magnetic field. This plate is provided with secondary electron catchers on both sides down field from where the beam strikes. Resolution of the slotted Faraday cup measurement is about one part in 240 (8% valley). The Faraday cup used to collect the H^- beam is water cooled and thermally

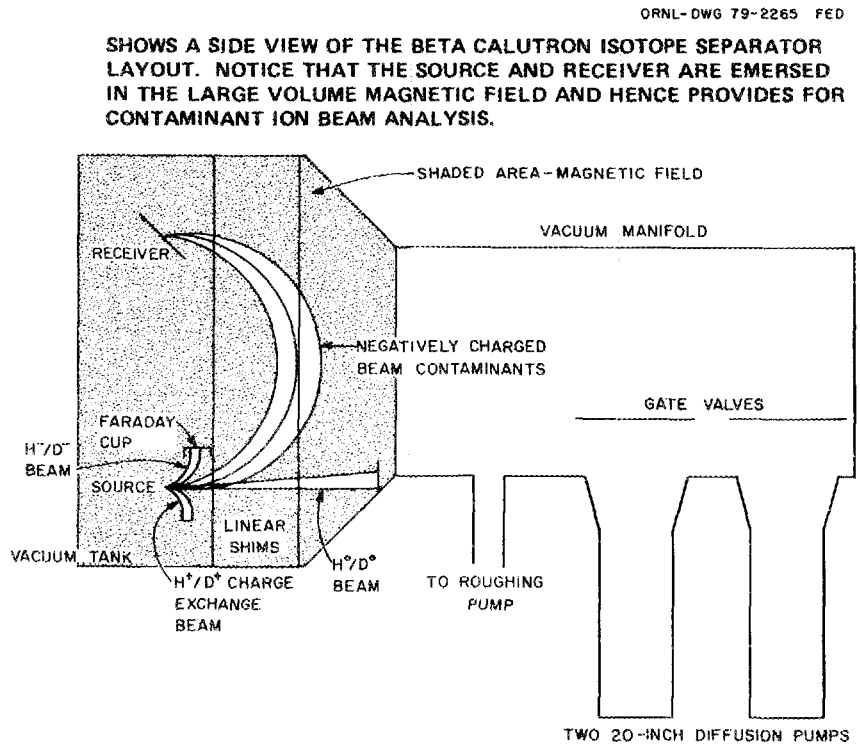

Fig. 17. Cross section of a beta Calutron tank.

isolated so that beam currents can be verified calorimetrically. Hydrogen gas is admitted to the arc discharge via two motor controlled, O-ring sealed needle valves through copper lines to the plasma generator. Polyvinyl chloride lines feed H_2 gas from the H_2 tank at ground through flowmeters and then provide high voltage insulation to connect to the needle valves, which are at high potential. Although the gas lines are purged with H_2 before hookup, no other measures are taken to reduce gas contaminants. Calorimetry is also used to check the electron recovery electrode and converter currents and is in agreement with them.

Arc filament power is provided by a three-phase copper oxide rectifier assembly with an output of 6 V(dc) and up to 400 A; the ripple is $\sim$4%. Arc power is provided by three independent steady-state supplies in parallel each rated at 10 A and 250 V(dc). A fourth such supply provides converter power. For the present purposes we can pulse each arc supply up to 60 s at 30 A at a 10% duty factor; arc supply outputs are manually balanced and adjusted by using primary induction regulators which make the induction regulator voltage of each supply equal and by using small ballast resistors on each supply. The arc ripple is <4%. Arc timing is accomplished from a master pulser using SCR switches in each of the arc power supply primary feeds; these SCR switches are in series with manual seal-in relay switches.

Figure 18 shows the high voltage power supply hookup. Both supplies as shown in Fig. 18 are rated for 1 A at 40 kV and dc operation. The electron recovery supply is unregulated with a 4% ripple and has been reconnected for 2-A steady-state operation at 20 kV. The accel supply voltage is regulated with a triode to 0.01% (short term) and can be emission limited to <100 mA during source conditioning to limit arc-downs. The high voltage stays on steady state and the arc is pulsed for running pulsed beams. High voltage turn-on is manual relay controlled.

G. Instrumentation

All beam current measurements in the dc mode are with calibrated panel meters or calibrated analog electrometer current meters for low currents of contaminants. For pulsed measurements and magnetic scanning of contaminants, a precision dropping resistor is used to supply the

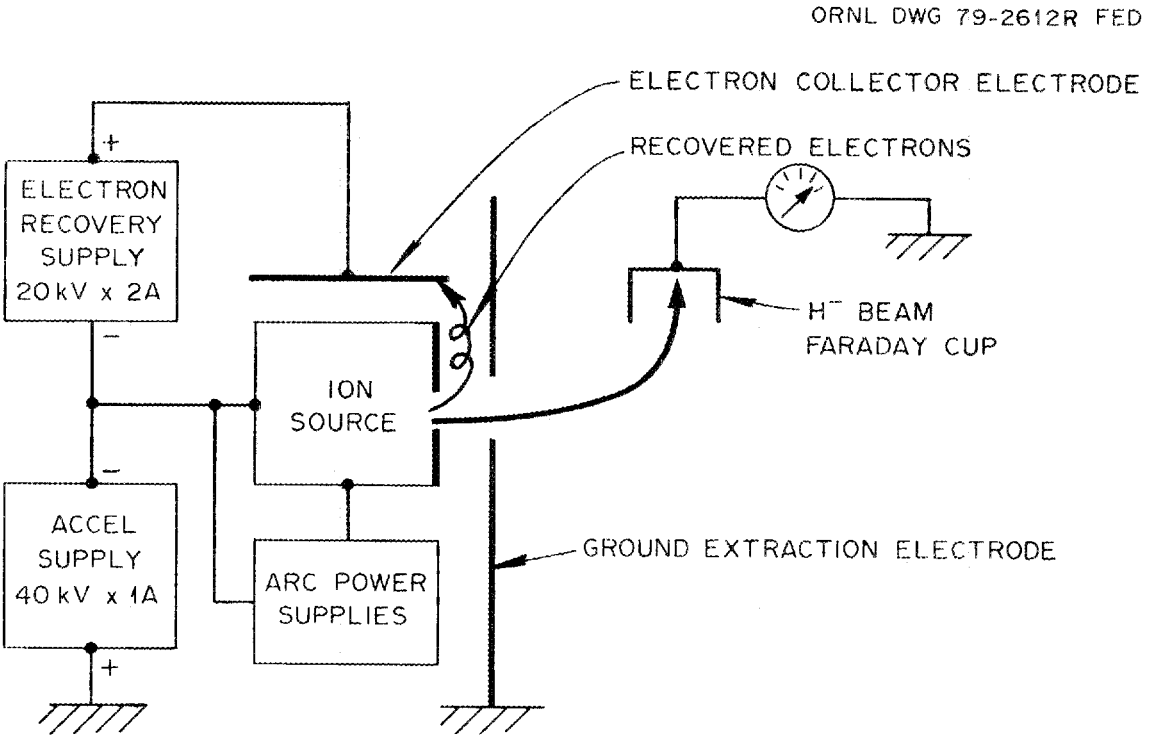

Fig. 18. Schematic diagram of the accelerating and electron recovery high voltage supplies.

oscilloscope input voltage. The mass scans are conducted by manually varying the motor-generator current to the magnet with the ion current voltage drop recorded by a digital oscilloscope, which can take 4×10^3 measurements per sweep. The magnetic field amplitude provided by a digital gaussmeter with analog output is recorded simultaneously on a second digital oscilloscope (digitized at fixed time intervals) channel. The full mass range was covered in several successive sweeps. Since the digital oscilloscope had only one part in 512 resolution, each mass range was swept several times at different oscilloscope preamplifier and electrometer gains to record both large and small peaks. Each sweep was recorded on a floppy disk cartridge for later analysis.

Arc current, arc voltage, electron recovery voltage and current, converter voltage and current, and accel supply current are sensed with Hall probe sensors or voltage dividers. The sensor voltage is converted to a digital pulse train with a frequency proportional to the voltage amplitude. The digital signals are converted to light pulses and are transmitted to ground over a light pipe system with 100-kHz full scale frequency and then reconverted to 0-10 V(dc) at ground. For dc operation, precision panel meters at high voltage are used also. Vacuum is measured with Bayard-Alpert gages, and hydrogen dc gas flow is measured with calibrated mass flowmeters for calculating gas efficiency; the dc gas flow with the arc off is used in the gas efficiency calculation.

II. EXPERIMENTAL RESULTS

A. H^- beam current and current density

Most of the data taken with emphasis on extracted H^- current has been with a 0.16- by 2.5-cm extraction slit, with a geometry shown in Figs. 8 and 9 in order to concentrate on increasing the extracted current density before attempting to scale up in total current. Although the very first experiments produced extracted current densities about 45 mA/cm^2 for >30 s and 60 mA/cm^2 for 100 ms, the values were not very repeatable. These early experiments[35] were "pulsed" either manually with a switch or by the arc supply overload circuit breaker. The latest experiments have had the arc pulse length and pulsing period controlled electronically; these experiments lead us to the conclusion that cesium coverage of the converter plate was one of our prime problems. By controlling the duty cycle (and hence converter plate and arc chamber temperatures), one can now reproducibly get extracted current densities of 56 mA/cm^2 at 23-mA total H^- beam. Figure 19 shows a reproducible, analyzed H^- beam pulse measured at the Faraday cup on a 15-cm radius after a 90° deflection. Beam transmission from the extraction slit to this Faraday cup has been measured as ∿80 ± 15%. With a 0.4-cm^2 extraction slit, one can calculate an extraction current density of

$$j_{H^-} = \frac{18 \text{ mA}}{(0.4 \text{ cm}^2)(0.80 \pm 0.15)} \approx (47\text{-}69) \text{ mA/cm}^2 .$$

These results can be reproduced by carefully controlling the duty cycle and, hence, average power loading on the uncooled converter plate; thus, the duty cycle is used to control the converter temperature.

Figure 20 shows an I_{H^-} trace for a condition of high accel current multiple breakdowns. Figure 20 also shows that I_{H^-} goes to zero even though I_{acc} ∿ 300-500 mA during breakdowns, which provides additional evidence that essentially no electrons are present in the I_{H^-} current reading from the Faraday cup.

RECENT RESULT FROM LONG PULSE STUDIES

ORNL-PHOTO 1579-82 FED

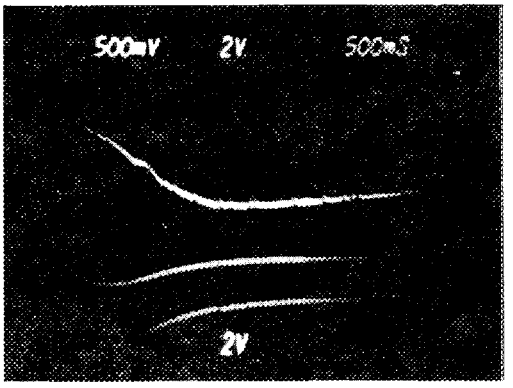

0

H^- CURRENT (5 mA/DIV)

ARC SUPPLY
1 AND 2 (5 A/DIV)

0

0

$V_{CONVERTER}$ ~ −150 Vdc AT 6A
P_{ARC} ~ 120 Vdc AT 15 A
0.4 cm^2 SLIT
V_{ACCEL} = 25 kV

Fig. 19. Oscilloscope trace of an analyzed, pulsed H^- ion beam.

ORNL-PHOTO 1580-82 FED

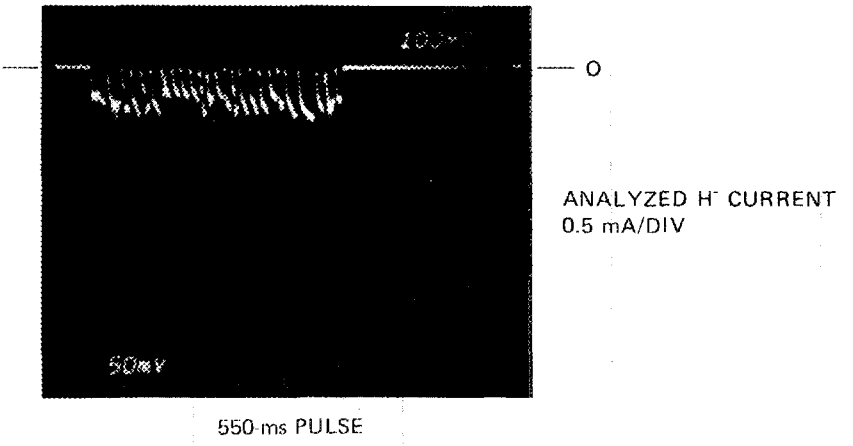

Fig. 20. Oscilloscope trace of the analyzed, pulsed H^- ion beam showing that I_{H^-} goes to zero during I_{acc} = 300-500-mA high voltage arc-downs of the source to ground.

B. H^- converter and converter materials

Our first experiments utilized the cesium-coated, flat molybdenum substrate H^- converter concept with the converter located behind the arc, which had been successfully used by the Russian[36] and BNL[37] groups. Figures 2, 3, 4, 7, 8, 9, and 10 show the placement of this converter in the present plasma generator. Initially, we used the cesium dichromate plus titanium reaction to generate elemental cesium. This method has been replaced by the use of elemental cesium dispensed from an oven for two main reasons: (1) heavy negative ion impurities were always a problem with this reaction, as discussed in Sec. II.G, and (2) the reaction was hard to control for long pulse work. Because the reaction is exothermal, the reactant mass and heat shielding must not be sufficient to let the reaction run away. The first experiments were run in a dc mode and successfully used 0.01-kg charges of $Cs_2Cr_2O_7$ with stoichiometric amounts of titanium powder. When the cesium dichromate charge was increased to .04 kg, the reaction proceeded violently once started and produced the damage to the source shown in Fig. 21. This reaction started with the tank vacuum at $\sim 4 \times 10^{-5}$ torr and proceeded with such violence that it expanded the stainless steel charge bottle ~10% [shown in Figs. 5 and 6] and blew off the accelerator electrodes, which are ~1.9- by 5-cm graphite cross section where they broke. To ensure that this occurrence was not repeated, we went back to .01-kg cesium dichromate charges plus titanium and evenly dispersed a 25% by weight quantity of pure sand in this mixture. No further trouble occurred before the mixture was abandoned for pure cesium feed.

Operation of the H^- converter is very sensitive to cesium coverage. The H^- production is nearly zero when there is no cesium. To investigate the effects of converter temperature and cesium coverage on H^- production, we operated the source in several modes. Because we cannot measure cesium coverage of the converter during source operation, we must infer cause and effect. Figure 22 shows an I_{H^-} trace where the converter voltage is turned on at low I_{H^-} current and presumably at very low cesium coverage. The current increases by ~15% for a converter voltage of ~100 V(dc). Figure 23 shows a similar trace at a higher

ORNL-PHOTO 4291-81

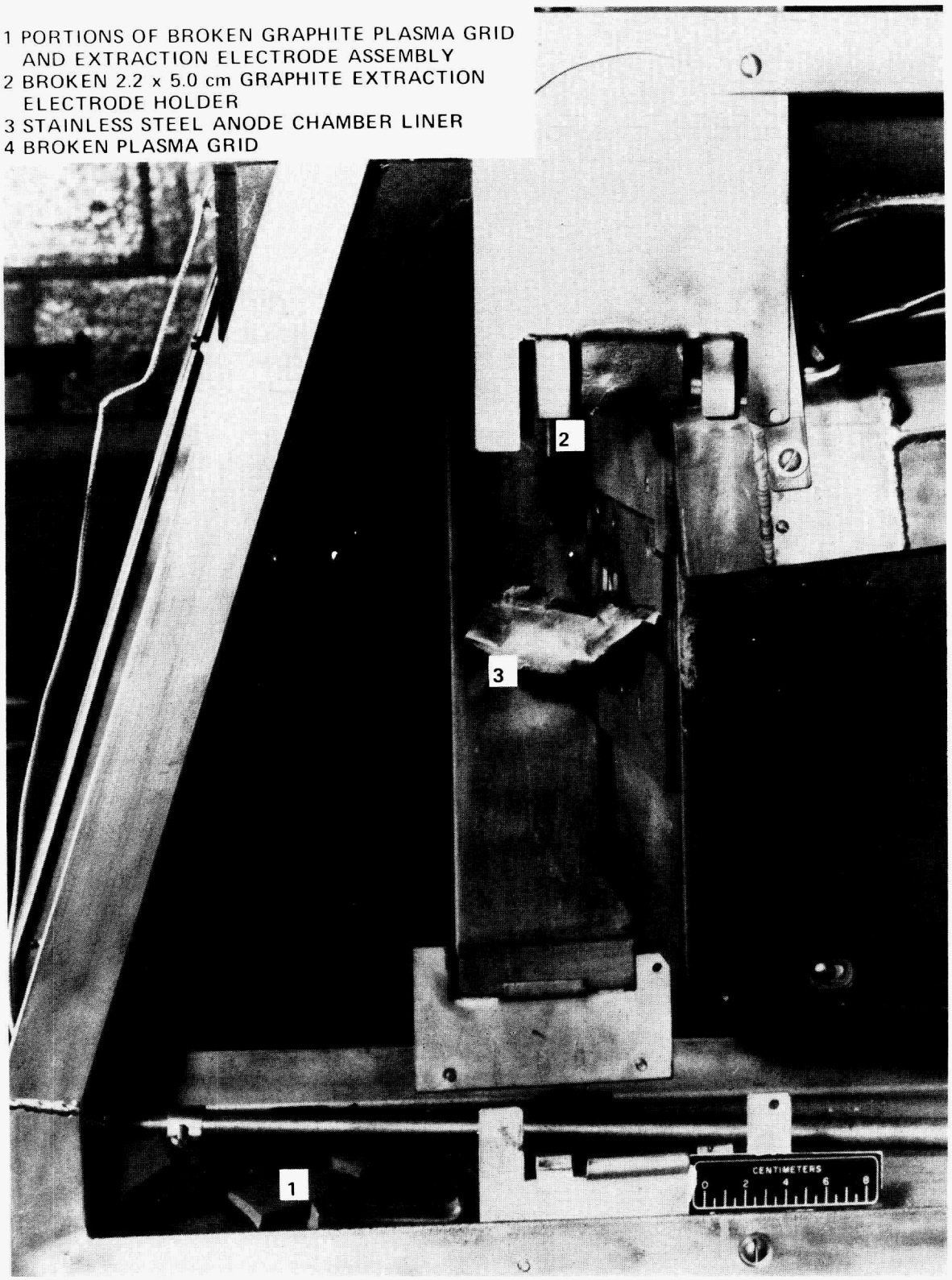

Fig. 21. Photo of the ion source showing damage from the violent cesium dichromate and titanium power reaction.

ORNL-PHOTO 1581-82 FED

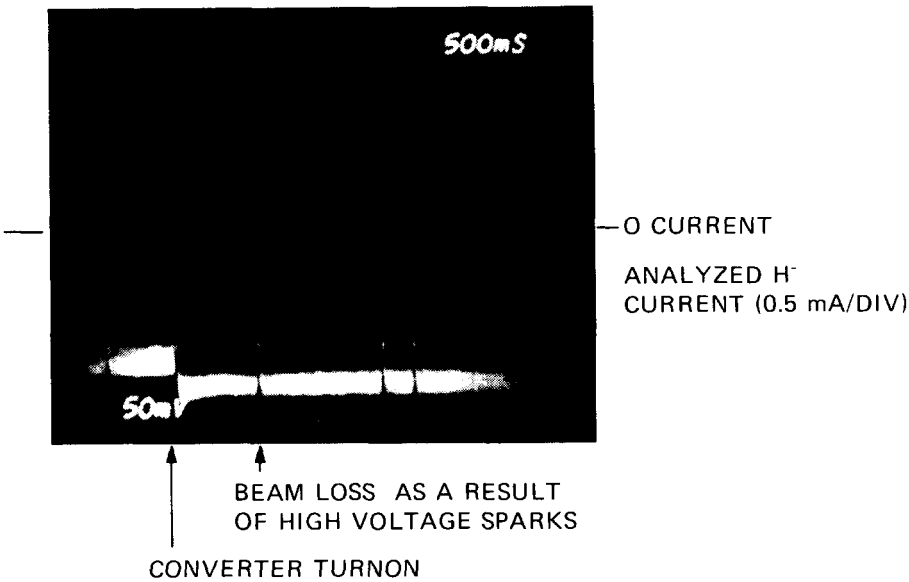

LOW CURRENT STEADY STATE BEAM OPERATION
B ~ 0.1 T

Fig. 22. Oscilloscope trace of the steady-state, analyzed H^- ion beam with the converter potential changing from floating to ∿-100 V(dc) during the recording with little change in the H^- ion beam.

ORNL-PHOTO 1582-82 FED

APPLICATION OF CONVERTER VOLTAGE PRODUCES LARGE INCREASE IN H^- OUTPUT

$H^- \rightarrow$ 2mA/DIV (ANALYZED)

$V_{CONVERTER} = -130$ V(dc)

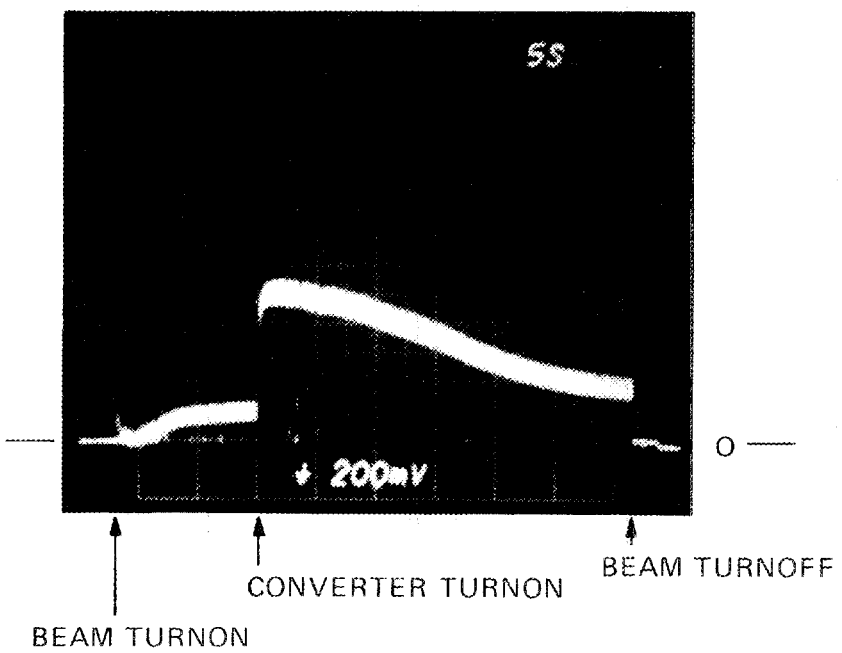

Fig. 23. Oscilloscope trace of the analyzed, pulsed H^- ion beam at more optimum converter cesium coverage and higher H^- ion (5-mA peak) current and a converter turn on to ∿-130 V(dc), which produces a 500% increase in the H^- current.

$I_{H^-} \approx$ 5-mA peak and presumably a more optimum cesium coverage. Here, the I_{H^-} increased by a factor of ∿5 when converter voltage was applied. From these we infer that over 80% of the extracted H^- ions come from the converter plate at high I_{H^-} current; the other 20% of the extracted H^- ions is from surface conversion on other surfaces. Earlier operation with no cesium produced very little H^- current (<0.1 mA), and from this we infer that volume production is an unimportant process for this source. Only solid molybdenum substrate material has been used in these experiments.

Figure 23 shows that after ∿5 s there is a decay of the I_{H^-} trace, which is attributed to a decay of the cesium coverage. At higher I_{H^-} currents (in Fig. 19), we see this decay beginning after ∿2.5 s. At a very low value of I_{H^-} = 1 mA, Fig. 24 shows an 8-s flat pulse. From these data we infer that controlling and maintaining cesium coverage on the molybdenum converter plate is important.

A series of experiments was run with a water cooled converter plate (both hot and cold), which resulted in much lower I_{H^-} currents. In all cases when the converter was examined after running, it was thickly coated with cesium oxide (490 K melting point) formed when the cesium coating oxidized upon exposing to air. Figure 25 shows a possible reason for the poor H^- yield from a calculation by Hiskes.[38] The H^- survival probability is almost one when emerging from a thin cesium layer, such as the 3/4 monolayer needed for minimum surface work function and maximum H^- current (shown in Fig. 26). Figure 25 shows a reduction in survival probability by approximately a factor of 10 for a thick cesium layer such as we had. Our maximum j_{H^-} was ∿2 mA/cm^2 for these cooled converter experiments; immediately upon returning to an uncooled converter, the j_{H^-} was high again at about 56 mA/cm^2. From this we conclude that temperature control of the converter plate will be necessary. However, the cesium feed rate has to be low enough and the temperature high enough not to produce thick cesium layers. Because the thick cesium layers were maintained during the cooled converter plate experiments (inferred from the low j_{H^-} yield and from the final thick layers), it should be possible to maintain cesium coverage for

ORNL-PHOTO 1583-82 FED

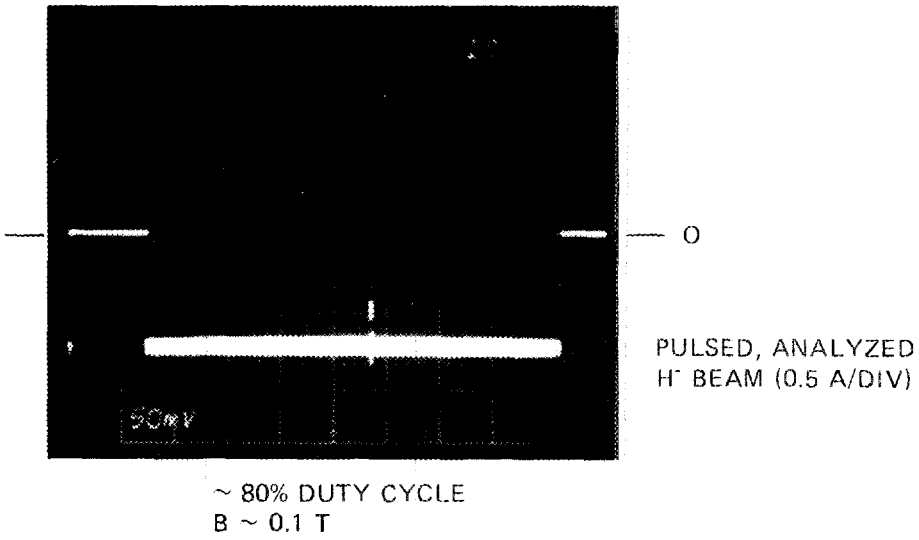

Fig. 24. Oscilloscope trace of an analyzed, pulsed H^- ion beam maintained constant over 8 s at 80% duty cycle and low beam current.

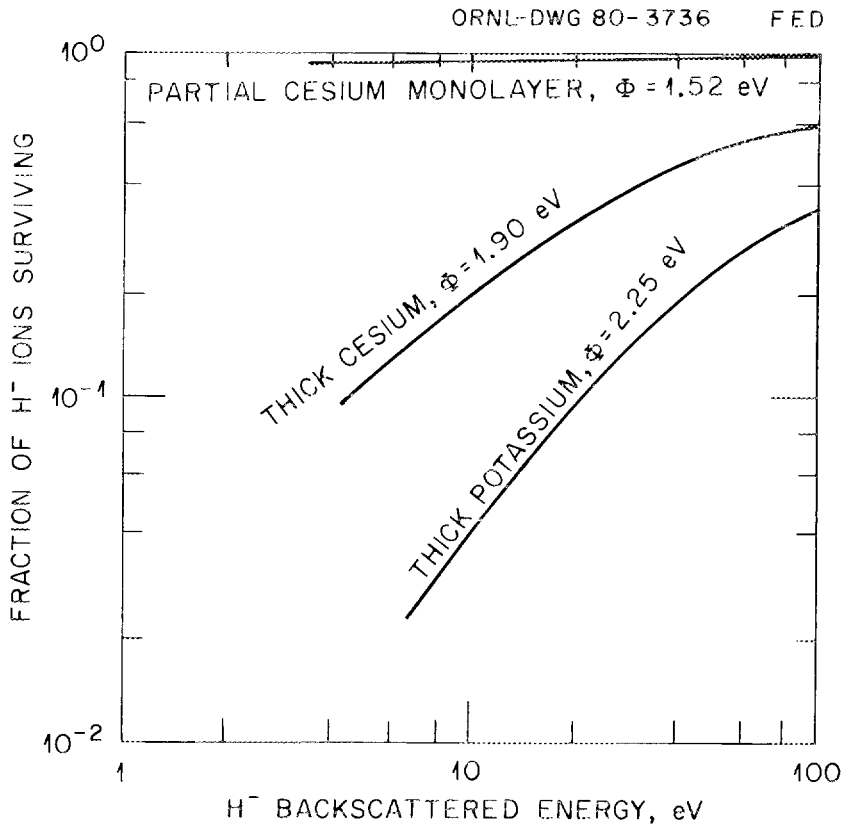

Fig. 25. Survival probability of H^- ions escaping from the converter surface as a function of cesium thickness on the converter and back-scattered energy [courtesy of J. R. Hiskes (38)].

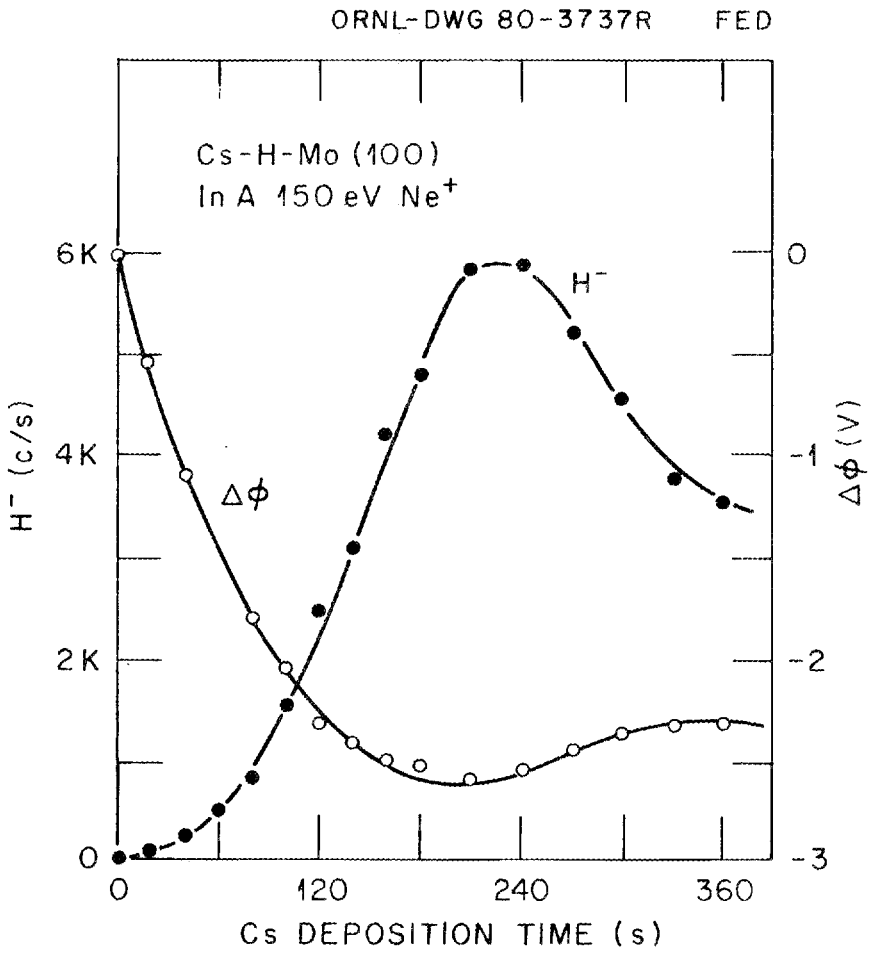

Fig. 26. Work function and H^- ion current as a function of cesium deposition time [courtesy of M. L. Yu, BNL 51304 (1980)].

long pulses of 30 s or dc operation for the present arc current densities. During one experiment that involved our uncooled molybdenum converter, we measured the net conversion efficiency (species mix unknown) of all positive ions as ∿13%; here we assumed the converter plate current to be due to H^+ impingement and to be spread uniformly over an area of arc ribbon width (∿1.27 cm). We subtracted a uniform I_{H^-}-current from this whole width, which would strike the back of the plasma electrode and as inferred from the analyzed extracted H^- current. The numerous destruction processes active while transporting the H^- ion from the converter to extraction slit have not been corrected for, but could raise this value since we are running at a H_2 pressure in the arc zone of ∿3 mtorr. Hiskes calculated that this surface conversion coefficient could be as high as 50%.[38] We have not established whether this effective conversion coefficient is dominated by the surface production process or by destruction processes in transporting the H^- ions to the extraction slit. At our present plasma parameters our estimate is that <5% of H^- ions leaving the converter will be destroyed and that the surface production process constitutes our main present limitation to achieving higher H^- currents and conversion efficiencies.

Negative ion beam current production in this source is currently dominated by the converter action when operating in the mixed cesium-hydrogen mode. With very small amounts of cesium on the converter, the H^- yield is not affected by converter potential, as demonstrated in Fig. 22. Figure 23 shows the large changes that typically occur when the converter is switched from an electrically floating mode at near arc potential to a driven mode at negative potential. From this we infer that most of the H^- ions come directly or indirectly via charge exchange from the converter when operating in the mixed cesium-hydrogen mode. Operation in the dc mode with 4-A, 150-V type arc discharges shows that the H^- beam current is roughly proportional to the converter potential up to about -60 V(dc), where an asymptotic region is entered. Converter voltage changes from -150 to -200 V(dc) cause an ∿10% increase in I_{H^-}. These results are clearly different from those reported by Prelec[29] on their Penning discharge with an emitter (same as a converter), in which no gain in I_{H^-} was seen in increasing the bias from floating to

-50 V(dc). The highest conversion efficiency that has been measured is ∿15%.[39] Power loading of the uncooled converter was 14 W/cm^2 for the above data.

C. Gas efficiency

The SITEX type H^- direct extraction source used the hot cathode arc discharge in these experiments. H_2 gas is introduced in the cathode cavity for initiating the arc discharge. Because the cathode is hot, a high gas pressure is not needed. Figure 3 shows a detailed view of the cathode area. By introducing the H_2 gas in the cathode cavity instead of the anode cavity, gas efficiency is raised about a factor of 2 for the short 2.5 cm slit. Present operation (as shown in Fig. 19) gives an atomic gas efficiency of 3%. Table I gives data for the best pulse used in this calculation.

Table I. Long pulse ion source parameters

Gas flow ∿0.063 Torr ℓ/s
I_{H^-} ∿18 mA (analyzed) ⇒ 23 mA (extracted)
Extraction slit = 0.16 × 2.54 cm^2
Arc current = 20 A
Arc volts = 100 V(dc)
Converter volts = 100 V(dc)
Converter current = 6 A
Flat converter electrode

Gas efficiencies approach zero as the cesium supply is lowered.

The cesium-hydrogen mixture in a magnetic field dominated discharge cannot be adjusted arbitrarily. Figure 27(a,b,c) shows H^- beam current time modulation caused by different arc conditions and that modulation is caused principally by power supply ripple and ionic sound phenomena. Ionic sound oscillation can be eliminated by increasing the gas pressure above a critical value. Under these conditions plasma generator

ORNL-PHOTO 1584-82 FED

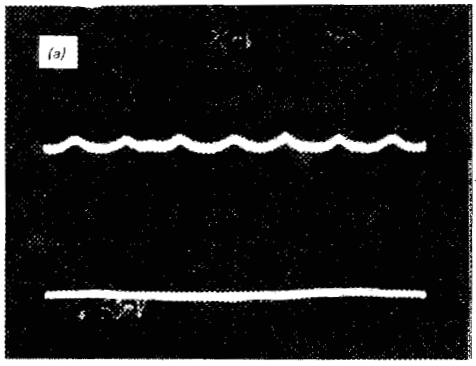

ANALYZED H^- BEAM CURRENT (0.5 mA/DIV.)
TOP TRACE (NO rf FILTER)
$V_{CONVERTER}$ = FLOATING
$I_{H^-} \approx 0.5$ mA
ARC = 120 V(dc) @ 9.2 A, dc OPERATION
$I_{acc} \approx 7$ mA
B ~ 0.14 T
CESIUM CARBONATE OVEN – 170 W

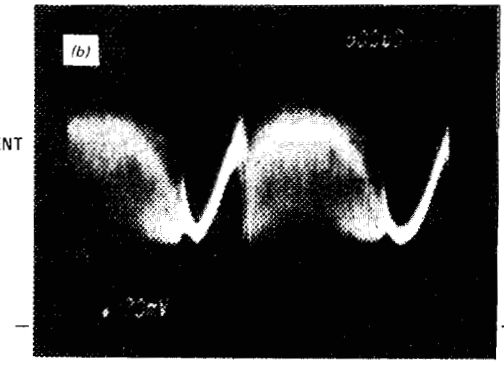

ANALYZED H^- BEAM CURRENT (0.2 mA/DIV.)
(NO rf FILTER)
CONVERTER = -50 V(dc) @ 0.5 A
$I_{H^-} \sim 0.8$ mA
ARC ~ 125 V(dc) @ 9.1 A, dc OPERATION
$I_{acc} \sim 39$ mA
B ~ 0.14 T
CESIUM CARBONATE OVEN ~ 170 W

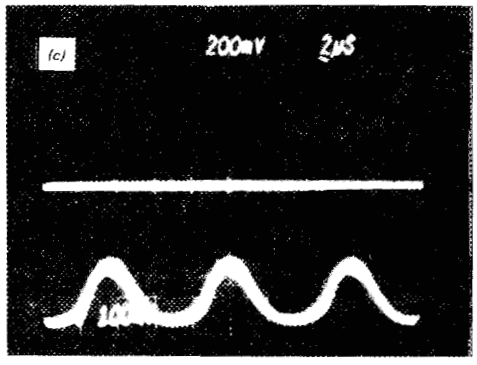

ANALYZED H^- BEAM CURRENT (0.2 mA/DIV.)
(NO rf FILTER)
CONVERTER -- FLOATING
$I_{H^-} \sim 0.8$ mA
ARC ~ 115 V(dc) @ 9.3 A, dc OPERATION
$I_{acc} \sim 7$ mA
B ~ 0.16 T
CESIUM CARBONATE OVEN OFF

Fig. 27(a,b,c). Oscilloscope trace of an analyzed H^- ion beam showing source oscillations with different source conditions.

reliability is 100% and conditioning is only needed to lower heavy mass negative ion impurities and lower outgassing to improve high voltage holdoff.

D. Electron control

Our H^- ion source experiments were designed for developing injectors for eventual reactor neutral beam use and, hence, were operated at seconds pulse length for tokamaks and at dc operation needed for mirror use. Reported values of extracted electron current to I_{H^-} current ratio elsewhere had been steadily reduced from values >450 in the early sixties[40] to present values of ∿0.5-2.[19]

Prelec,[19] Kelley,[41] and the Russian group[42] reported trouble with electron control on their ion source systems or concepts. Because most of the experimental work to date has been with a few millisecond pulses, they have yet to experience the full damage these currents can cause when collected at full acceleration energies. We designed an electron recovery structure that collects ≳99% of extracted electrons at 5-10% of the extraction gap energy,[33,43] which permits us to design the arc geometry without unnecessary concern for extracted electron currents and to concentrate on other problems such as gas efficiency, etc. Earlier, long pulse and dc operation without this recovery system with our ion source resulted in melted water cooled structures due to the concentrated nature of these currents (shown in Fig. 13). Recent operation with the electron recovery system has shown evidence of greatly reduced high voltage breakdowns and no concentrated dumped power due to efficient collection of these electrons.[20]

Figure 14 shows the electron recovery system we designed and built for the H^- SITEX source, which employs cross field extraction. Any H^- source that uses cross field extraction can use this system with slight geometry changes. Electrons and H^- ions are extracted from the plasma grid slit by the extraction electric field $\vec{E}$. Negative hydrogen ions and electrons are separated by $\vec{E} \times \vec{B}$ forces with the ions typically following 15-cm-radius trajectories for the present experiments and electrons following cycloidal trajectories up the front of the source.

These ∿1.8-mm vertical amplitude electron cycloidal trajectories are followed and feed ≳99% of the extracted electrons onto the top of the source between the anode and recovery electrode. Figure 16 shows evidence of these cycloidal electron trajectories. Above the slit is a series of darker lines that are about the same length and parallel to the extraction slit. Their origin is not understood. However, the spacing between these images corresponds to the electron cycloidal cusp period for this magnetic and electric field.

Once inside the recovery electrode regions, a slight E_z field is created parallel to the magnetic field lines and away from the source center, which dumps these electrons onto the electron recovery electrode. It is important that E_z be approximately zero until the electrons are well into the recovery electrode region. Figure 13 shows the first model where E_z was created before the electrons were fully in the electron recovery electrode region. Figure 15 shows the shaped electrode used to dump the recovered electrons on the recovery electrode; Fig. 28 shows a more detailed view of the electron dump geometry. The potential on the electron recovery electrode can be varied from +0.4 kV to +25 kV with respect to source potential. Figure 29 shows the efficiency with which the electron recovery electrode system collects electrons when used with the maximum length ion exit slit of 12.7 cm. For low arc currents, the collection efficiency is ∿100% above V_{ec} = 1.5 kV (electron collector bias with respect to source accel potential). For higher arc currents, there is an optimum V_{ec}. For 9.5 A of arc current, V_{ec} should be 2.5 to 3 kV at which point the electron collection efficiency is ≳99.5%. This system has been tested up to I_{ec} = 1-A dc conditions by using abnormal gas feed conditions to generate this electron current.

An important and very visible effect of the efficient electron collection is the greatly reduced high voltage sparking rates. With our recent experiments, we put ∿60% of the power supply energy into the I_{H^-} = 18-mA beam as analyzed after 90° of deflection and a 23-cm path length.

Further parameteric studies were made of the electron recovery process. Figure 30 shows I_{ec} versus magnetic field for all other parameters held constant. The $1/B^2$ dependence of the electron current

ORNL/DWG/FED 78-1073

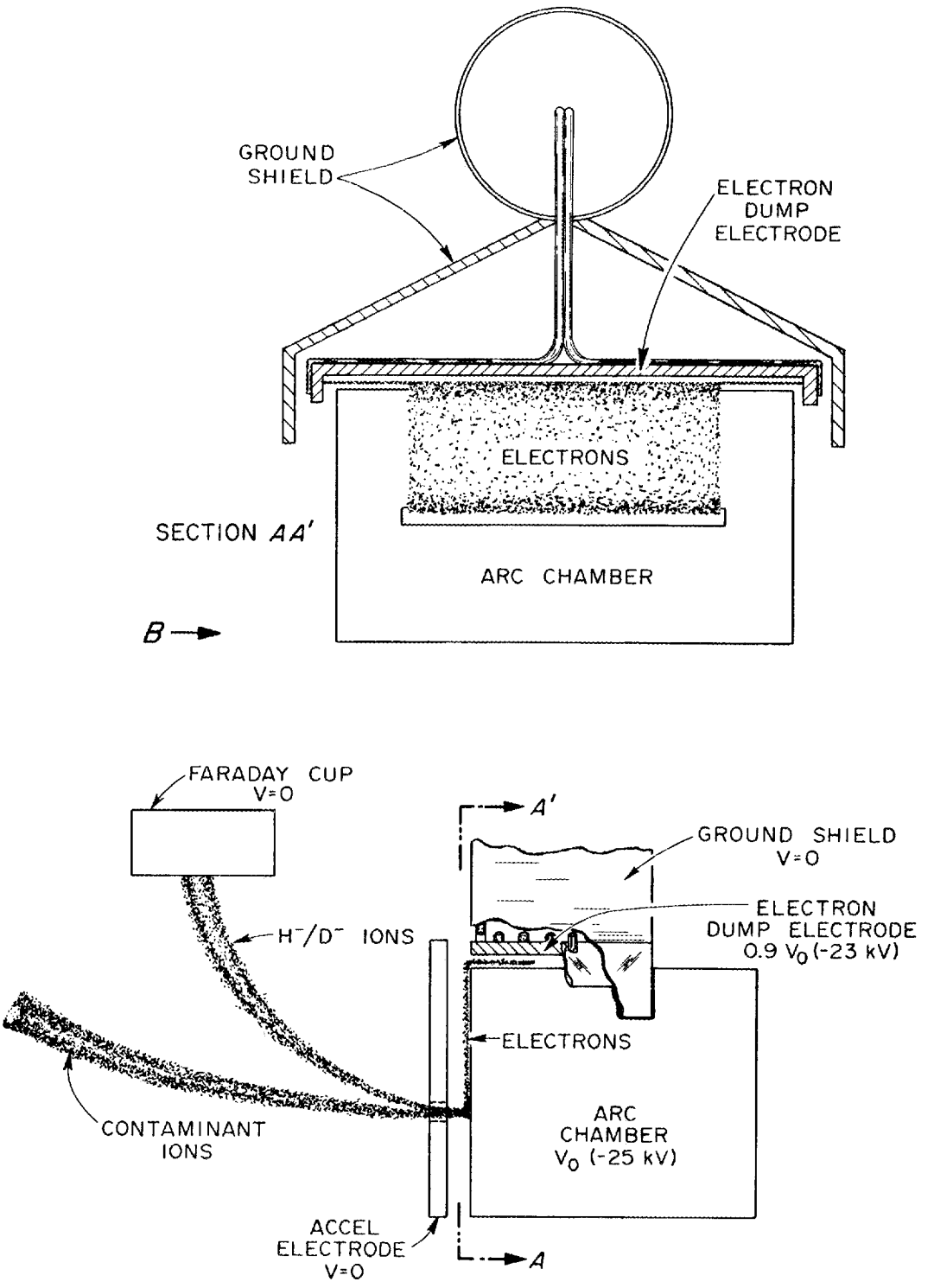

Fig. 28. Side and top view of the electron recovery geometry.

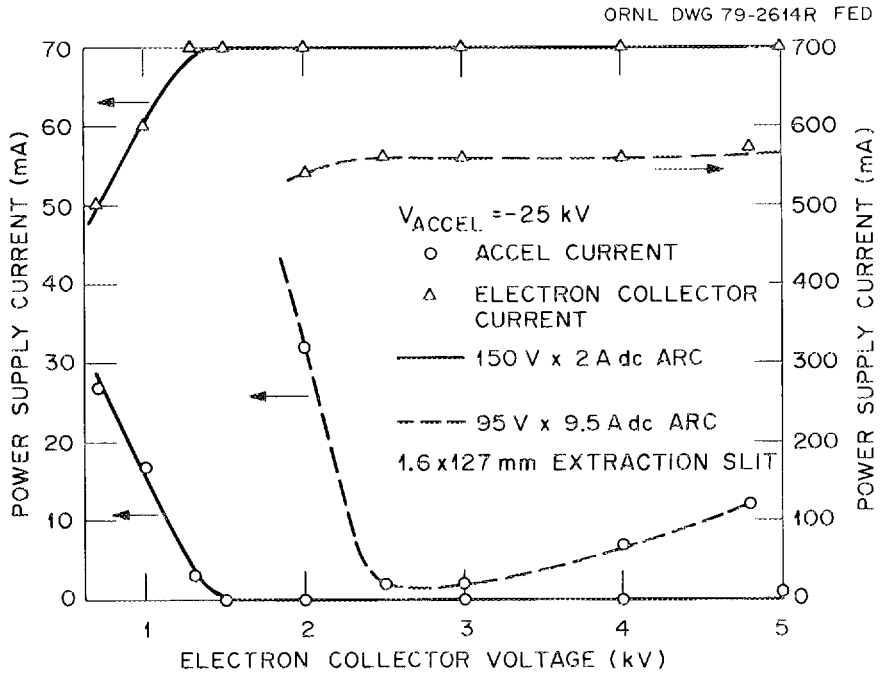

Fig. 29. Electron collection efficiency vs electron collector bias from plasma generator accel potential.

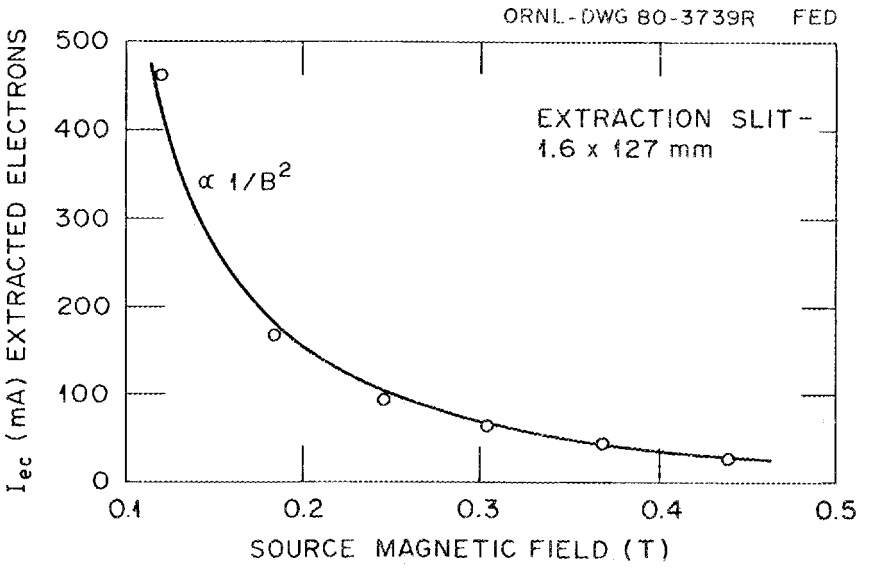

Fig. 30. Recovered electron current (=extracted electron current) vs magnetic field with abnormal arc operation to generate this electron current.

I_{ec} shows clearly that this current is dominated by collisional diffusion processes in the arc, which have this form for diffusion perpendicular to $\vec{B}$. Since previous measurements on arcs of this type have shown an exponential decay of n_e with distance from the arc column, we can decrease the magnitude of I_{ec} by moving the primary arc further away from the extraction slit. This has been confirmed on earlier tests with Cl^- beams with this type of arc discharge.

E. Long pulse/dc operation

The principal problem with the present source for long pulse and dc operation is that most of the plasma generator and electrode structure is uncooled. When high current operation is attempted, the graphite parts get hot enough to simply sublimate away. The molybdenum converter plate has been above 1809 K during steady state operation, as evidenced by melted stainless steel fastening screws; this same experiment also melted the stainless steel screws holding the electron reflector electrode to its insulator. Clearly a long pulse or dc source must have adequate heat removal during arc operation and be maintained hot enough during off periods to prevent cesium condensation.

We made several limited measurements for long pulses at low duty cycle. Figures 31 and 32 show a 20-s beam of $I_{H^-} < 4$ mA; the figures also show that turn-on conditions can vary greatly depending presumably on cesium conditions. Figure 33 shows a similar trace for 40 s with $I_{H^-} < 5$ mA. The I_{H^-} increase then decrease shows the complex effects of increasing converter temperature and increasing cesium supply due to arc power at unmatched rates. Figure 34 shows $I_{H^-} \sim 4$ mA for a 45-s pulse and the effect of increasing the arc current in the middle of the pulse. Figure 35(a,b) shows the I_{H^-} trace with the arc turned completely off during a 50-s pulse. Then we can see that I_{H^-} comes back on at substantially the turn-off value indicating that long thermal time constants are involved. We infer from this that cesium coverage of the thermally floating converter did not change substantially during the off time. Earlier, dc operation with either a hot or cold water cooled converter ($\sim$363 K and 298 K) consistently produced low currents and a converter

ORNL-PHOTO 1585-82 FED

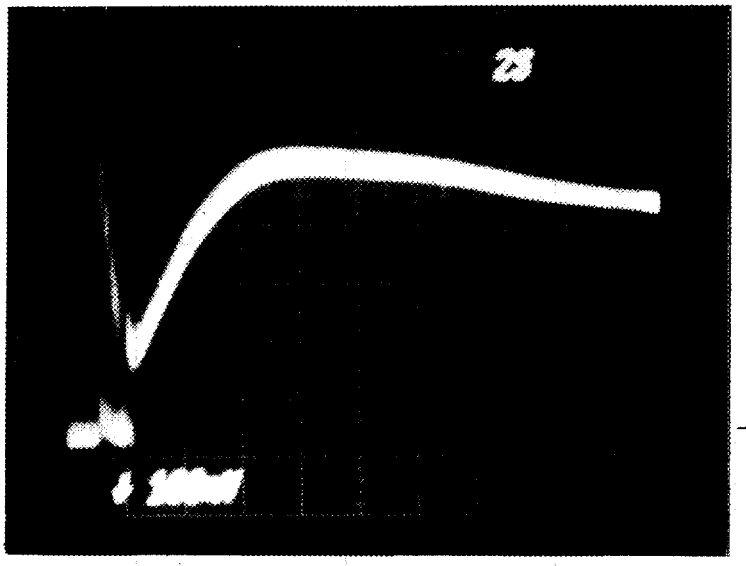

ANALYZED H^- BEAM CURRENT (1.0 mA/DIV.)
MULTIPLE ARC BREAKER KICKOFFS NEAR
FRONT OF PULSE
$I_{H^-} \approx 4$ mA
CONVERTER -150 V(dc) @ 1.5 A
ARC ~ 140 V(dc) @ 7 A, PULSED,
(OFF FOR 5 MINUTES)
$I_{ec} \approx 30$ mA (HAS ELECTRON RECOVERY)
B ~ 0.15 T
CESIUM CARBONATE OVEN ~ 400 W

Fig. 31. Oscilloscope traces of an analyzed, pulsed H^- ion beam for $I_{H^-} \leqslant 4$ mA at 20 s showing a large turn-on H^- ion current.

ORNL-PHOTO 1586-82 FED

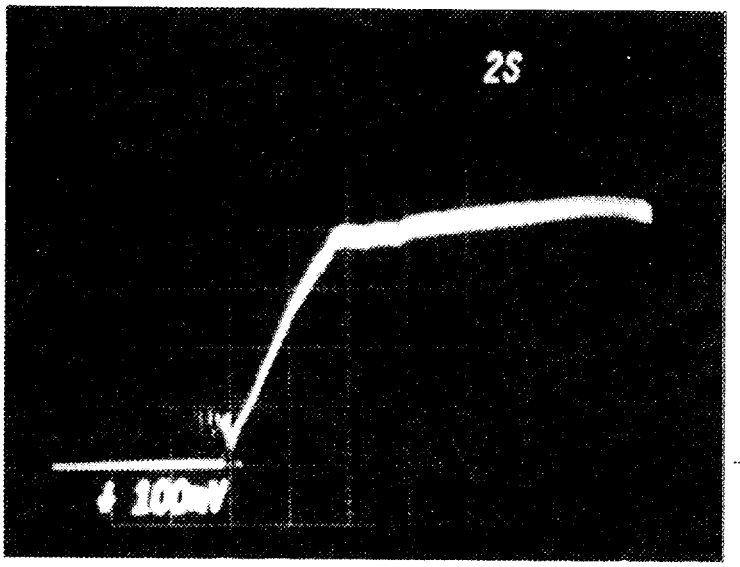

0

ANALYZED H^- BEAM CURRENT (1.0 mA/DIV.)
$I_{H^-} \sim 4$ mA
CONVERTER -120 V(dc) @ 1.5 A
ARC ~ 125 V(dc) @ 9.2 A, PULSED,
(OFF FOR ~10 MIN.)
$I_{ec} \sim 45$ mA (HAS ELECTRON RECOVERY)
B ~ 0.15 T
CESIUM CARBONATE OVEN ~ 430 W

Fig. 32. Oscilloscope traces of an analyzed, pulsed H^- ion beam for $I_{H^-} \leqslant 4$ mA at 20 s showing a small turn-on H^- ion current and subsequent rise.

ORNL-PHOTO 1587-82 FED

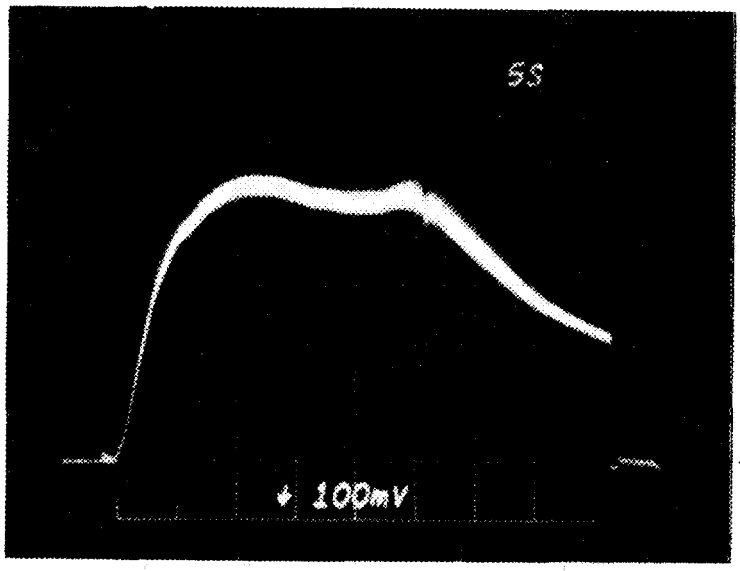

0

ANALYZED H^- BEAM CURRENT (1.0 mA/DIV.)
$I_{H^-} \sim 4$ mA
CONVERTER -120 V(dc) @ 1.2 A
ARC ≈ 110 V(dc) @ 6.6 A, PULSED,
(OFF FOR 5 MINUTES)
$I_{ec} \approx 45$ mA
B ~ 0.15 T
CESIUM CARBONATE OVEN ~ 430 W

Fig. 33. Oscilloscope trace of an analyzed, pulsed H^- beam for $I_{H^-} < 5$ mA and for 50 s showing a near zero turn-on H^- ion current.

ORNL-PHOTO 1598-82 FED

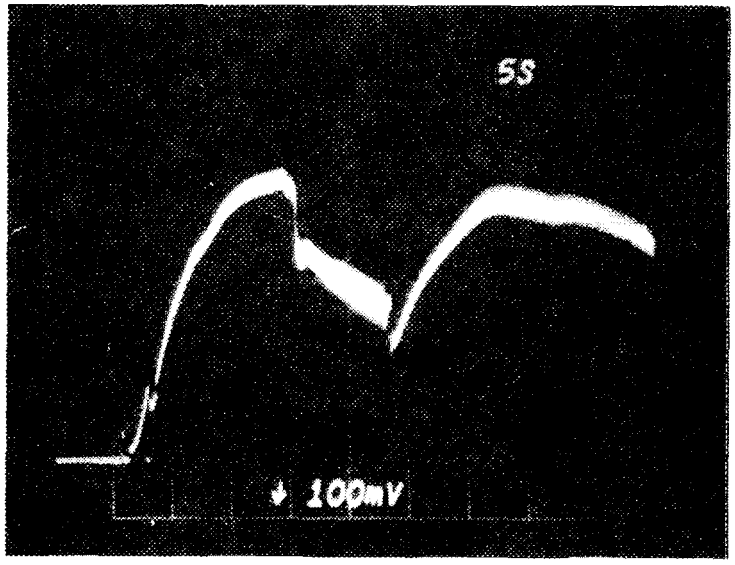

ANALYZED H^- BEAM CURRENT (1.0 mA/DIV.)
$I_{H^-} \approx 4$ mA
CONVERTER -120 V(dc) @ 1.2 A
ARC ≈ 110 V(dc) @ 6.6 A (AT ~13s
AFTER ARC TURNON AT 6.6 A
TWO MORE ARC SUPPLIES
INCREASED ARC TO ~20 – 30 A.
BACK TO 6.6 A AT τ = 23 s)
$I_{ec} \approx 45$ mA
B ≈ 0.15 T
CESIUM CARBONATE OVEN ~ 430 W

Fig. 34. Oscilloscope trace of an analyzed, pulsed H^- ion beam for $I_{H^-} \sim 4$ mA and 50 s showing a sharp H^- ion current fall with the arc current approximately doubled between 13 s and 23 ms during the pulse.

ORNL-PHOTO 1589-82 FED

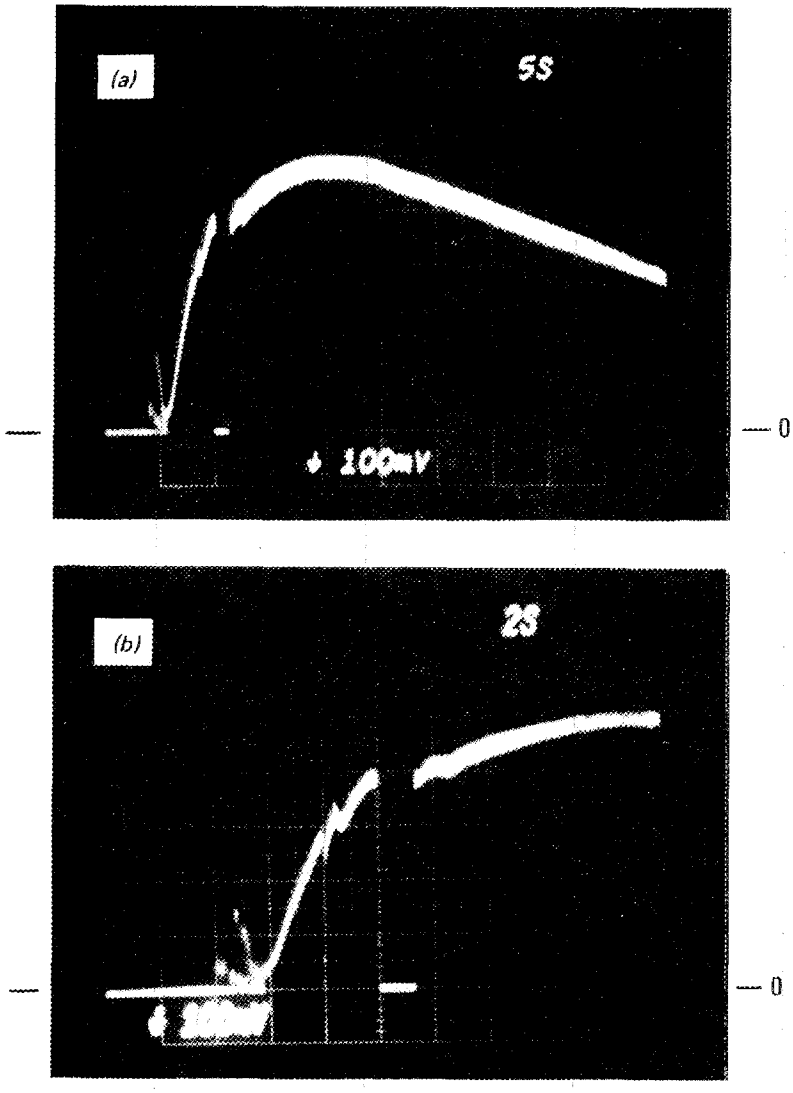

ANALYZED H^- BEAM CURRENT (1.0 mA/DIV.)
$I_{H^-} \approx$ 5 mA
CONVERTER -120 V(dc) @ 1.2 A
ARC ≈ 110 V(dc) @ 6.6 A
(AT 5 s ARC OFF FOR 1.3 s)
PULSED ON AFTER 20 m
CESIUM OVEN – 520 W
I_{ec} ~ 45 mA
B ~ 0.15 T
CESIUM CARBONATE OVEN ~ 520 W

Fig. 35(a,b). Oscilloscope trace of an analyzed, pulsed H^- beam showing the effect of turning off the arc momentarily during the pulse and that the beam current recovers to approximately the same value.

that was thickly covered with cesium when pulled for inspection. From these results obtained at 10-A arc currents, we may be able to find a suitable higher temperature where almost optimum cesium coverage can be maintained.

For the extraction geometry of Fig. 10(a,b), using an uncooled extraction grid, we have sustained some melting of the molybdenum slit during operation. Long pulse and dc operation will require water cooled electrode structures.

F. Optics

We measured the average optics of this H^- source during operation by examining the diffusion pump oil decomposition pattern left by the H^- ions on the water cooled, copper Faraday cup at the 90° deflection angle some 23 cm from the source[20] (see Fig. 8 for this setup). The burn pattern (using uniform magnetic field trajectories) corresponds to $\theta_\perp = \pm 4°$ (perpendicular to the exit slit). A complete profile scan has not been performed. In our interpretation of the burn pattern, we have assumed a Gaussian profile and that the edge of the burn pattern corresponds to less than 5% of the beam intensity. We can visually see burn H^+ patterns on the same type of surfaces resulting from charge exchange reactions, which correspond to beam intensities less than 1% of the total extracted beam. From these assumptions the $\theta_\perp(1/e) \sim 2\pm1°$ and $\theta_\parallel(1/e) \sim 1\pm1°$ (parallel to the slit direction). The extraction slit has been cut on a 30° angle as shown in Fig. 10a, which reduces the end effects of the short slit. No electrode heat loadings or instantaneous beam optics have been measured. This pattern corresponds to extraction current densities of 56 mA/cm^2 and 23-mA total H^- beam.

G. Impurities

Measurements made on extracted H^- beams by other groups[44] have shown beam impurity levels on the order of 10% or more. The best results by LBL using a small mass spectrometer are recently much lower; these measurements are from a 300-V self-extracted beam.[45] C. C. Tsai of ORNL

reports 10-50% impurities on the duoPIGatron negative ion source as measured with an $\vec{E} \times \vec{H}$ Wein filter on 1-keV beams.[46] Early measurements with the SITEX source showed similar high contamination results. These SITEX source measurements were made using the magnetic field in which the source operates, which acts as the momentum filter and yields whole beam analysis.[47] In order to reduce these impurities, we vacuum outgassed the graphite structures and plasma sprayed them with a 0.05-0.10-mm thick layer of M_o. After installing and obtaining a 1×10^{-5} torr vacuum, we used the ion source heaters to further vacuum outgass the structure. This is then followed by pure H_2 arc operation to further condition the structure. Heavy mass negative ion beams were low over the mass range of 15 → 20 amu at 100 V and 5 A arc power with normal pure H_2 arc operation. As soon as the cesium dichromate reaction started, however, we were up to impurity levels of 10 to 50% of the beam. Figure 36 shows the impurity current for the sum of masses 15 through 20 and the H^- beam current as a function of time for dc operation after the oven temperature was raised. Earlier operation with the oven empty and oven heater on showed that these impurities cannot be coming from the oven assembly without at least the presence of cesium. Even after extended operation, the level is nearly 10% of the beam. Figure 37 is a mass scan of impurities obtained during low power dc operation of the source using residual cesium in the arc chamber. The spectrum is dominated by ^{12}C and $^{16-18}O$; OH^- is clearly low compared to ^{16}O. The higher mass impurities are assumed to come from backstreaming Convoil 20 organic diffusion pump oil (used in early experiments) cracking products. The diffusion pumps had a water cooled baffle. We estimate that the mass distribution of ions is not affected by more than 30%, due to changing the source magnetic field during these scans and the spectrum has not been corrected for this effect.

Our most recent results have been obtained using elemental cesium feed and have consistently shown reduced heavy mass negative ion contaminants by approximately a factor of 5.[20] Figure 38 shows the results of measurements made during the first operation with elemental cesium after a careful outgassing procedure, as outlined earlier. We see that

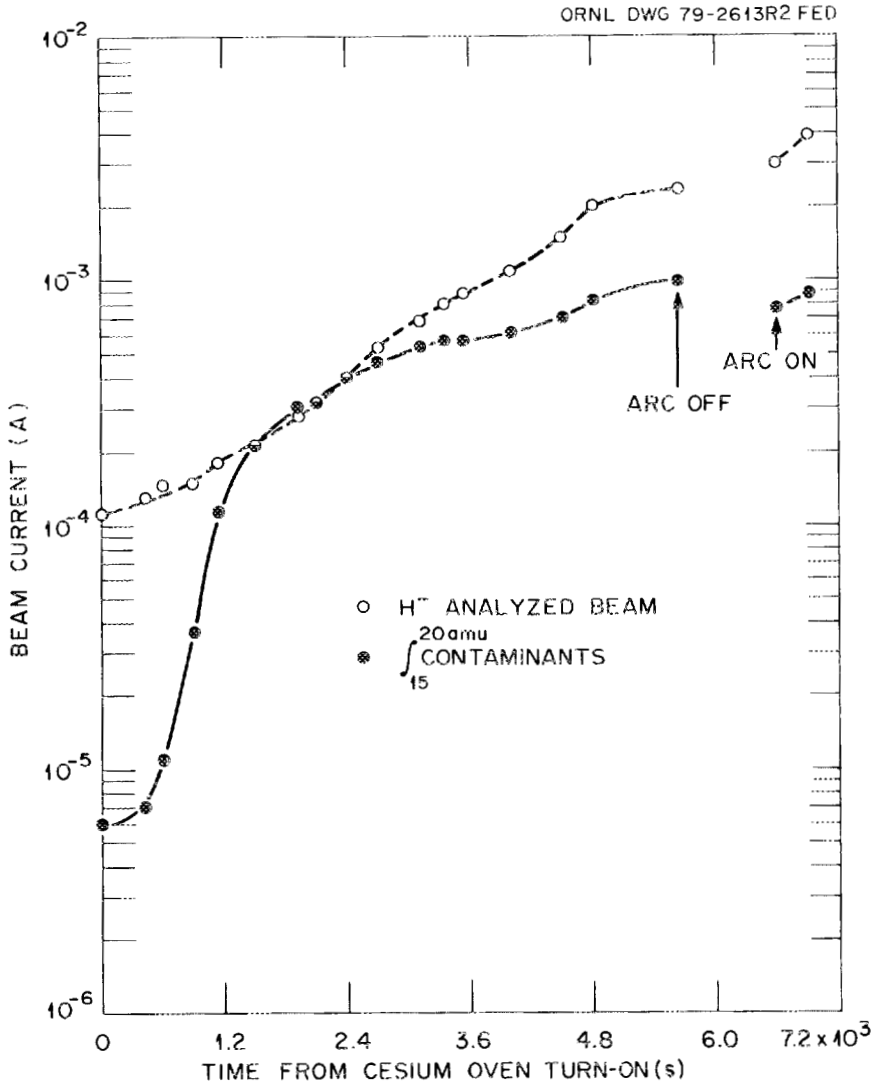

Fig. 36. Heavy mass impurity level sum over the 15- to 20-amu range and analyzed H^- beam current as a function of time (after source outgassing and H_2 mode arc conditioning) from the cesium dichromate oven turn-on and for dc operation.

ORNL-DWG 79-2266R FED

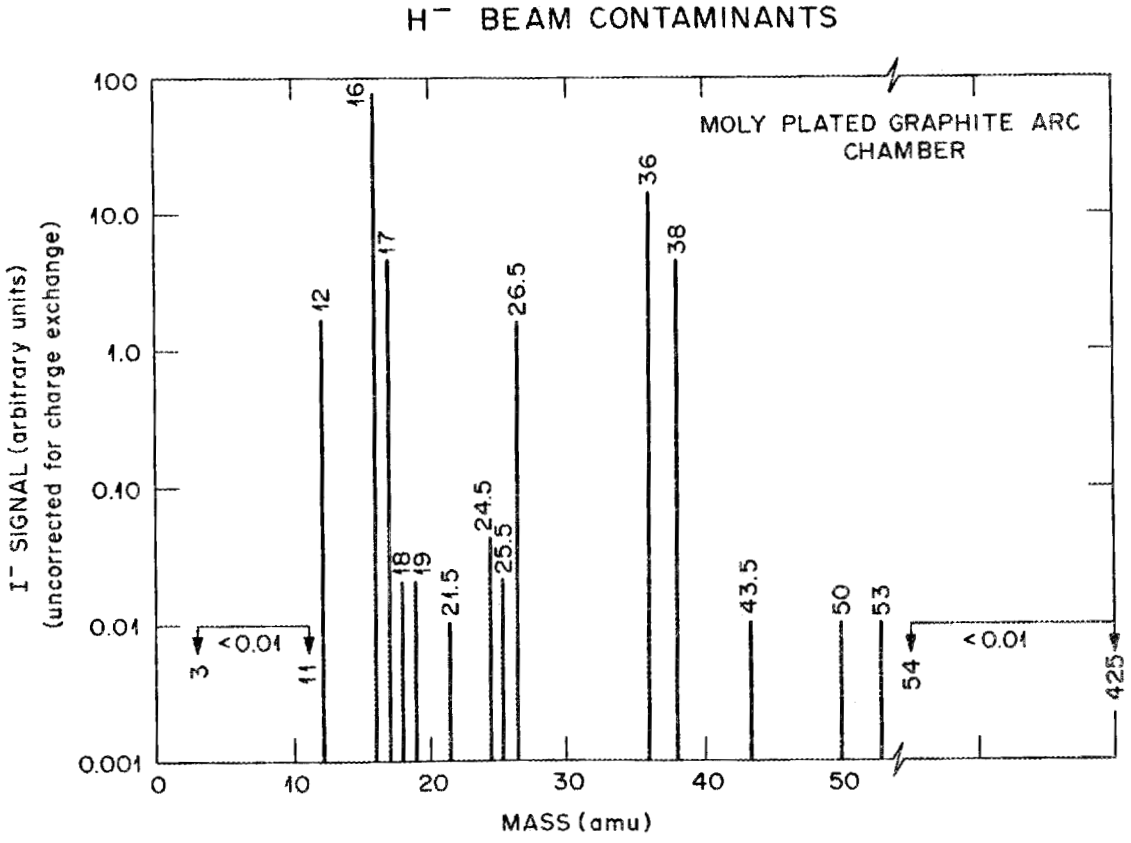

Fig. 37. Full mass impurity spectrum (Fig. 36 includes part of the impurities plotted in Fig. 37) with the oven off and using residual elemental Cs for H^- ion generation.

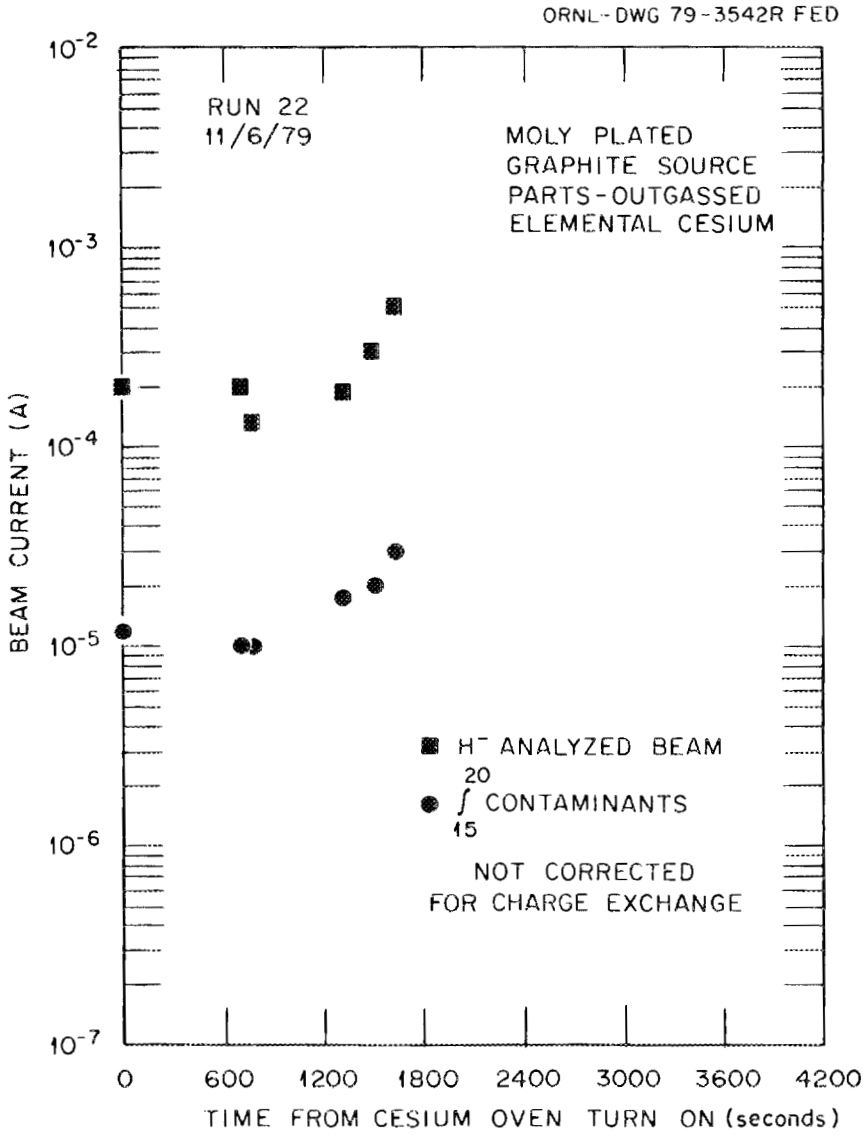

Fig. 38. Heavy mass impurity level sum over the 15- to 20-amu range and analyzed I_{H^-} as a function of time from the beginning of elemental cesium admission (after heater outgassing and H_2 mode arc conditioning) and for dc operation.

the heavy mass negative ion contaminants never exceed 10% of the H^- beam for low power arc operation. Figure 39 shows a contaminant mass spectrum obtained using the elemental cesium. Again, ^{12}C dominates the spectrum. Extended high power arc operation can produce much larger $^{12}C^-$ beams due to the hot graphite subliming and reacting with H_2 gas. We can see in Fig. 39 that small Ne^{20-22} negative beams are present (used as mass markers) with perhaps a $^{9}Be^{12}C^-$ contaminant. The ^{9}Be and ^{12}C peaks are definitive mass markers.

We changed to Santovac-5 diffusion pump oil and refrigerated diffusion pump baffles just before this experiment, and this may account for the changed heavier mass spectrum from that shown in Fig. 37, which we attribute primarily to the diffusion pump oil. Spectra in Fig. 39 were obtained using two 2-channel digital oscilloscopes to simultaneously record both the magnetic field (being scanned), the high resolution mass Faraday cup, and the upper half integral mass plate ($\sim$2.6 amu wide at mass 16). Figures 40 and 41 show a typical portion of a mass spectrum (ion current versus sample time) and the high resolution that was available with the Faraday cup and the integral mass spectrum. At a given magnet current (point in time), the magnetic field was read from the second channel to compute the mass.

The upper and lower half integral mass plates normally continuously monitor the mass 15- to 20-amu region with H^- in the collection Faraday cup (see Fig. 42). The lowest contaminant levels have been obtained using elemental cesium along with careful source conditioning. To accomplish the measurement, the magnetic field was varied so that the integral mass plates covered the range from 10 to 20 amu with resulting total beam impurities over this mass range of $\sim$0.5%. Also since Fig. 39 shows that mass contaminants heavier than 20 amu constitute $\lesssim$10% of the contaminants we can safely say that total contamination can be reduced to <1% of the beam by the use of elemental cesium and careful source conditioning. The mass distribution of contaminants will vary during source conditioning. In nongraphite sources with cryopumping we expect the ^{12}C peak to be greatly diminished. Impurities other than carbon produced by the present source can be kept below 1-2% after only modest conditioning.

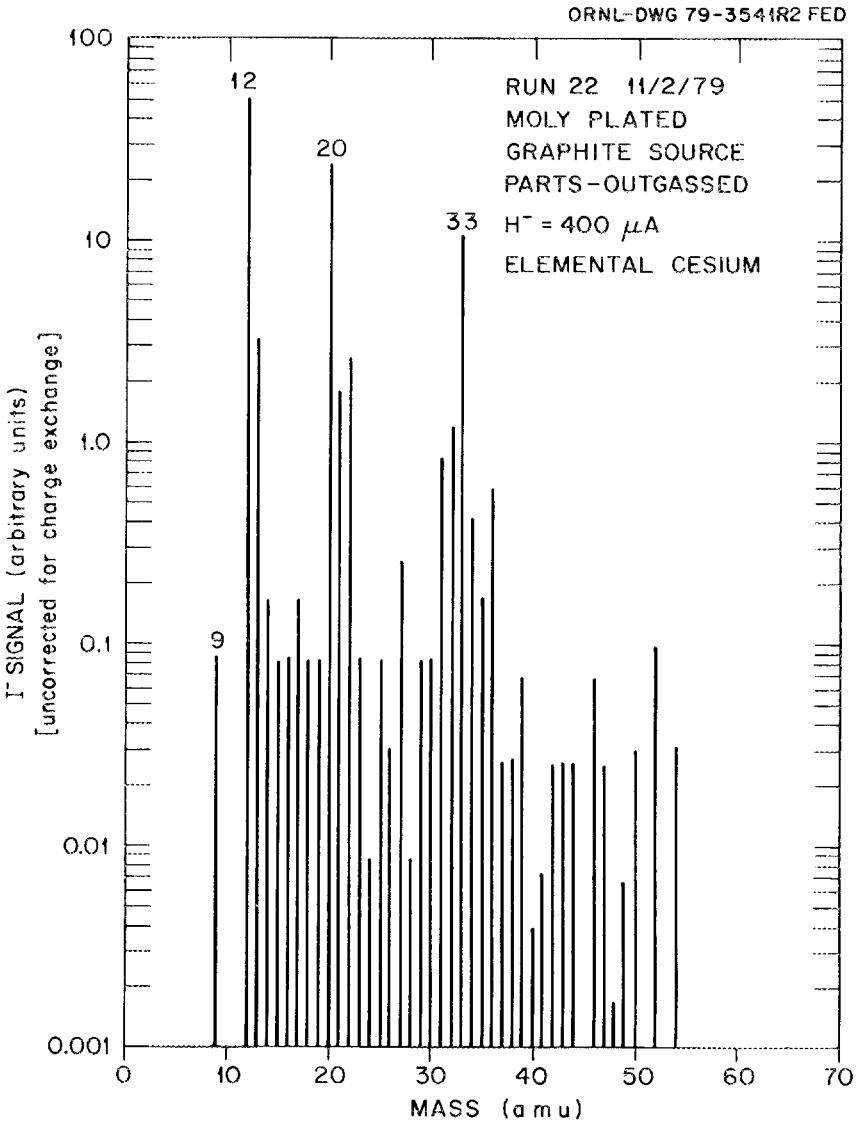

Fig. 39. Full mass impurity spectrum that includes the impurities plotted in Fig. 38.

ORNL-PHOTO 1590-82 FED

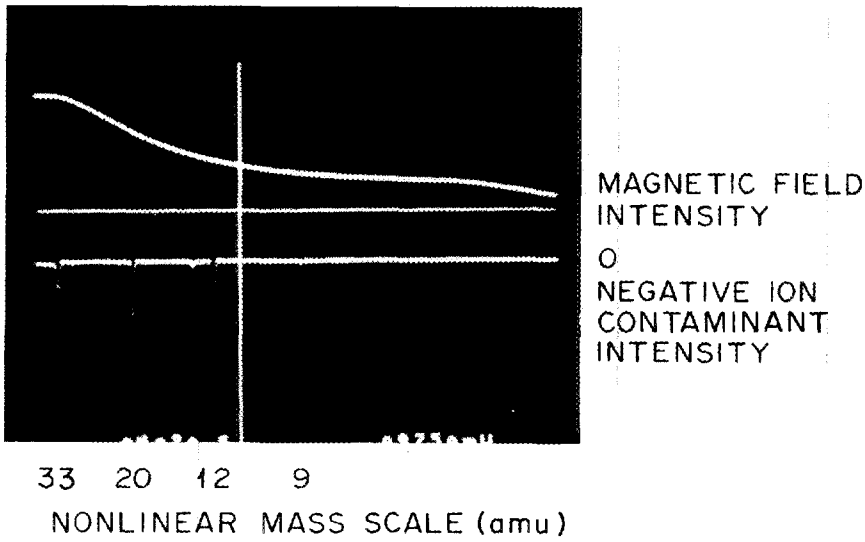

Fig. 40. Portion of the digital oscilloscope spectra from the high resolution, heavy mass Faraday cup used in gathering the data for Fig. 38.

ORNL-PHOTO 1591-82 FED

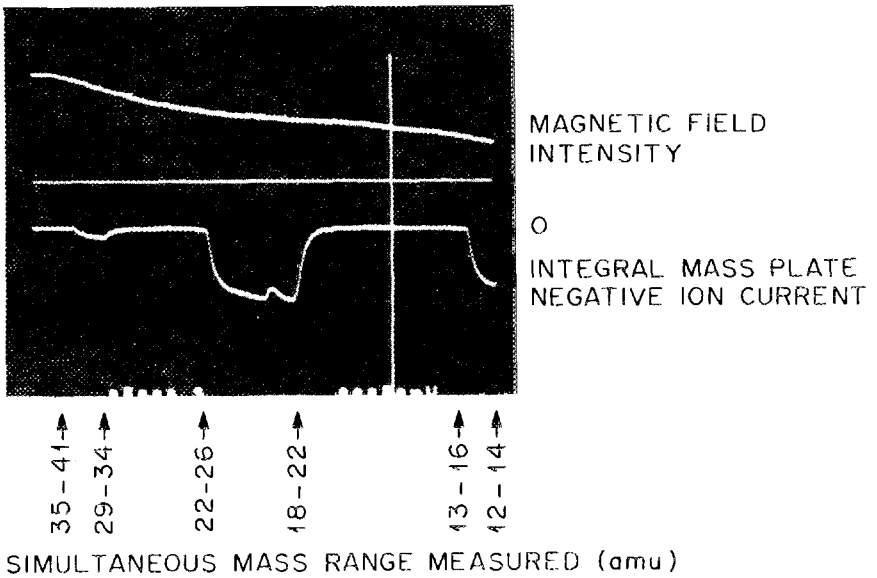

Fig. 41. Portion of the digital oscilloscope spectra from the integral mass collection plate collected simultaneously with the high resolution data of Fig. 40.

ORNL/DWG/FED 78-659R

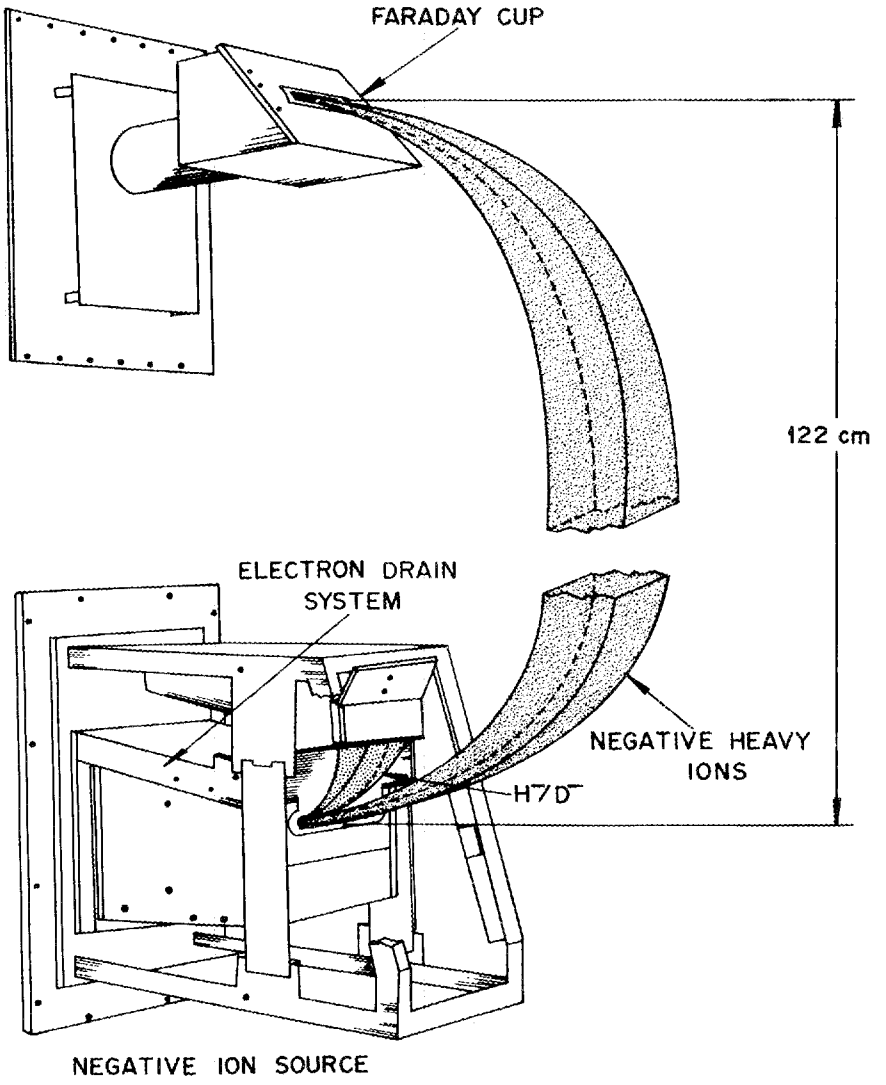

Fig. 42. Illustration of the H^- and negative ion contaminant beams and beam measurement Faraday cup.

III. DISCUSSION

A. Error analysis

In this section we present an error analysis of our measurements to show that they are sufficiently accurate to guide source development. The most fundamental measurement is the H^- analyzed ion current, which fortunately is our most reliable measurement. Discussions in Sec. II.A have shown that the extracted electron current is effectively separated from the H^- beam by the $\vec{E} \times \vec{B}$ fields. In addition, the H^- Faraday cup has a guard shield around it and is completely immersed in the 1-kg magnetic field so that electrons are prevented from entering it and secondary electrons generated by the beam cannot escape (see Fig. 8). No electrode electric fields exist at the H^- Faraday cup entrance; hence, any electrons that entered the cup as a result of flow along the beam plasma would be at low energy. We calorimetrically measured the H^- beam current and found that it agreed with the current measurement to within ±5%, which is about the present limit of our calorimetry and current measuring accuracy. Our present estimate of analyzed H^- beam current error is ±5%, both for the dc beam measurements and the pulsed measurements using oscilloscopes and precision current resistors.

The test stand instrumentation was described in Sec. I.H. Gas flow, high voltage, and magnetic field systems were calibrated and were accurate to ±5%. Accuracy of the Hall probe current sensor system measurements, as transmitted to ground via the voltage-to-frequency light pipe system, depends on the amplitude of the signals. These signal measurements are accurate to about ±10% at their present levels. At low signal levels, the hysteresis of the Hall probe sensors can become significant, leading to much larger errors. The hysteresis according to the manufacturer is ±1/2% of the sensor full scale value.

B. Plasma generator

Although we have not measured the source species mix, we estimate that the molecular mix of positive ions in the plasma ribbon is higher than 50%, a fact which could be important in our estimates of converter

efficiency since H^+ to H^- conversion efficiency η is a sensitive function of nucleon velocity. The detailed functional effects of H_2^+ and H_3^+ have not been measured, but could be significant in explaining η as a function of converter voltage and arc current, because the species mix may change with arc current as it does in other sources.[48] The n^+ densities necessary to produce the observed H^- fluxes are about 3.5×10^{12} cm^{-3} at an ion temperature of about 0.2 eV. The 100-eV, fast H^- ion flux density is $n_f^- = 1 \times 10^{10}$ cm^{-3}. The fast electron density is $n_{fe} \gtrsim 2.4 \times 10^{11}$ cm^{-3}. Assuming a 5 eV electron temperature, the Debye length under such conditions is

$$\lambda_D \sim 743 \frac{(5\ \text{eV})^{1/2}}{(3.5 \times 10^{12})^{1/2}} = 8.9 \times 10^{-4}\ \text{cm} \quad .$$

Thus, since the converter sheath thickness is small compared to the arc dimensions, positive hydrogen ions (either atomic or molecular) drift into the converter plasma sheath and experience a 100-eV component of velocity normal to the surface added to the other small velocity components. One thus expects an approximately normal surface collision. The converter surface consists of the molybdenum substrate with adsorbed cesium and hydrogen atoms. The interaction of the fast hydrogen particles with the surface has been discussed by several authors. The conversion of hydrogen atomic particles to H^- ions is essentially independent of the initial charge state for the velocities considered. In the water cooled converter experiments, which resulted in thick cesium coverages, we demonstrated the sensitivity of the process to the correct cesium coverage. The details of the conversion of fast hydrogen particles to negative ions involve sputtered adsorbed hydrogen atoms, reflected hydrogen projectiles, and thermally desorbed particles. Details of these processes must be studied under much closer, controlled conditions than in the present studies. Outgoing H^- ions from the surface experience the 100-eV normal energy gain from the plasma sheath, which is added to the reflected energy (equal to or less than the incoming energy) or sputtered energy.[49]

C. H^- loss mechanisms

Negative hydrogen ions leaving the converter sheath must transverse the arc column and associated gas plume before extraction. For the present data source pressure was $\sim 3 \times 10^{-3}$ torr. For 100 eV H^- ions $n\sigma_{-10}\ell = 0.056$ producing a 5% production of slow H^- ions from the reaction

$$H^- + H^0 \rightarrow H^0 + H^- \text{ (slow)} .$$

The following is a list of H^- neutralization reactions along with the fraction of H^- ions produced by the converter which are lost.

$e + H^- \rightarrow H + 2e$	0.4% loss
$H^- + H^+ \rightarrow H + H$	2.3% loss
$H^- + H_2 \rightarrow H + H_2 + e$	1.1% loss

Thus, we see that for the low power arc operation used that the H^- loss mechanisms from the converter to extraction slit sum to <4%. Operation at 8×10^{-3} torr would produce 14% slow H^- ions by charge exchange and $\sim$10% H^- loss. Negative hydrogen ion loss to electron stripping during acceleration depends on the gas pressure (and hence gas efficiency of the source), accelerator column length, and beam energy. Preliminary measurements of our stripping losses after single gap extraction and deflection through 90° along a 23-cm path is 20 ± 15%. Higher gas efficiencies would clearly be desirable to keep stripping losses in the accel column low.

D. Comparison of surface conversion negative ion sources

Table II shows a comparison of our results with the results of other surface conversion negative ion neutral beam development groups. Our development started in the 2- to 30-s pulse range, since this may be the most difficult range to achieve flat, reliable beam pulses and for which the applications to neutral beam heating of plasmas are now required.

Table II. Comparison of surface conversion negative ion sources

	SITEX	DuoPIGatron	BNL	LBL	Russia
Pulse length (s)	5	0.1	0.01	dc	0.001
Extracted j_{H^-} (mA/cm^2)	56	<20	2200	10	3300
Total beam current (mA)	23	<500	600	>400	1000
Gas efficiency (%)	3[a]	(Est 3-5%)	6[b]	NA	5
Pressure (anode) (mtorr)	∿3	∿4	∿100	∿1	∿100
Beam energy (keV)	25	1 keV	15	0.3	NA
Beam impurity (%)	<1[c]	≲10	<10	∿1	∿10
I_e/I_{H^-}	4-6	0.1	0.5	NA	>>1
Electron current recovery (%)	>99	0	0	0	0
Optics $\theta_\perp$ (1/e) (°)	2 ± 1	NA	12	NA	NA
Arc efficiency (kW/A)	110[d]	∿100	8	8	18

[a]Flat converter.

[b]Cylindrically focused converter.

[c]Measured at low arc power and small H^- beams.

[d]Arc 5 times longer than extraction slit (slit = 2.5 cm).

From these results we see that considerable work is needed on the plasma generator and beam accelerator before negative-ion-generated neutral beams can provide practical heating for tokamak and mirror fusion experiments.

The reliability of the SITEX plasma generator is 100% at this power level and can be estimated to run hundreds of hours. Further research into higher gas efficiency, long pulse converter control, optics, and all metal cooled source operation is under way. Future parametric studies will include moving the primary hydrogen discharge back from extraction slit, which should greatly reduce the I_e/I_{H^-} ratio without affecting j_{H^-} significantly. Our upcoming plans also include testing the scalability of this source.

ACKNOWLEDGMENTS

The authors wish to acknowledge the many valuable suggestions from members of the Plasma Technology Section of the Fusion Energy Division. The technical discussions with Drs. G. D. Alton of the Physics Division, G. G. Kelley, consultant, and C. C. Tsai and J. H. Whealton of the Fusion Energy Division were particularly useful. The mechanical designs were by V. Lunsford of Union Carbide Engineering Division and construction supervision and innovation by H. T. Milton of the Isotopes Separation Section of the Chemical Technology Division. Power supply modification designs were by G. M. Banic, also of the Isotopes Separation Section. Instrumentation designs were by R. Wright of the Fusion Energy Division and D. Thompson of Union Carbide Engineering Division and calibrations were by D. Sparks of the Fusion Energy Division. The program support and technical discussions of Dr. H. H. Haselton of the Fusion Energy Division continue to be vital to the program.

REFERENCES

1. H. Eubank, R. Goldston, V. Arunasalam, M. Bitter, K. Bol, D. Boyd, N. Bretz, J.-P. Bussac, S. Cohen, P. Colestock, S. Davis, D. Dimock, H. Dylla, P. Efthimion, L. Grisham, R. Hawryluk, K. Hill, E. Hinnov, J. Hosea, H. Hsuan, D. Johnson, G. Martin, S. Medley, E. Meservey, N. Sauthoff, G. Schilling, J. Schivell, G. Schmidt, F. Stauffer, L. Stewart, W. Stodiek, R. Stooksberry, J. Strachan, S. Suckewer, H. Takahashi, G. Tait, M. Ulrickson, S. von Goeler, M. Yamada, C. Tsai, W. Stirling, W. Dagenhart, W. Gardner, M. Menon, and H. Haselton, Proc. 2nd Joint Grenoble-Varenna Int. Symp. on Heating in Toroidal Plasmas (1980).
2. H. Eubank, L. R. Grisham, T. A. Kazub, H. Kugel, G. Schilling, N. B. Williams, and the PLT and PDX Experimental Groups, Phys. Rev. Lett. 43, 270 (1970).
3. L. A. Berry, C. E. Bush, J. D. Callen, R. J. Colchin, J. L. Dunlap, P. H. Edmonds, A. C. England, C. A. Foster, J. H. Harris, H. C. Howe, R. C. Isler, G. L. Jahns, H. E. Ketterer, P. W. King, J. F. Lyon, J. T. Mihalczo, M. Murakami, R. V. Neidigh, G. H. Neilson, V. K. Paré, D. L. Shaeffer, D. W. Swain, J. B. Wilgen, W. R. Wing, and S. J. Zweben, Proc. 6th Int. Conf. on Plasma Physics and Controlled Nuclear Fusion Research (Berchtesgaden, 1976), Vol. 1, p. 49 (1977).
4. M. Murakami, D. W. Swain, S. C. Bates, C. E. Bush, L. A. Charlton, J. L. Dunlap, G. R. Dyer, P. H. Edmonds, A. C. England, H. H. Haselton, J. T. Hogan, H. C. Howe, D. P. Hutchinson, R. C. Isler, T. C. Jernigan, S. Kasai, H. E. Ketterer, J. Kim, P. W. King, E. A. Lazarus, J. F. Lyon, C. H. Ma, J. T. Mihalczo, J. K. Munro, A. P. Navarro, G. H. Neilson, D. R. Overbey, V. K. Paré, M. J. Saltmarsh, S. D. Scott, J. Sheffield, J. E. Simpkins, W. L. Stirling, C. C. Tsai, R. M. Wieland, J. B. Wilgen, W. R. Wing, R. E. Worsham, and B. Zurro, 8th Int. Conf. on Plasma Physics and Controlled Nuclear Fusion Research, IAEA-CN-38 (1980).
5. L. C. P. Henger, Proc. 8th Symp. on Engineering Problems of Fusion Research, IEEE 79CH1441-5NPS, p. 831 (1979).

6. INTOR Group, in Report of the International Tokamak Reactor Workshop, Zero Phase (STI/PUB/556), IAEA, Vienna (1980).
7. Engineering Test Facility Design Center Newsletter, ORNL, February 1980.
8. R. R. Borchers and C. M. VanAtta, The National Mirror Fusion Program Plan, Lawrence Livermore National Laboratory Report UCAR-10042-80 (1980).
9. B. A. Prichard, Jr., R. Little, D. E. Post, and J. A. Schmidt, in Proc. Symp. on the Production and Neutralization of Negative Hydrogen Ion Beams, Brookhaven National Laboratory Report BNL-50727 (1977).
10. L. D. Stewart, in Proc. Symp. on the Production and Neutralization of Negative Hydrogen Ion Beams, Brookhaven National Laboratory Report BNL-50727 (1977).
11. J. W. Stearns, K. H. Berkner, and R. V. Pyle, Proc. 2nd Topical Meeting on the Technology of Controlled Nuclear Fusion, Vol. 4, p. 1221 (1976).
12. M. M. Menon, C. C. Tsai, D. E. Schechter, P. M. Ryan, G. C. Barber, R. C. Davis, W. L. Gardner, J. Kim, H. H. Haselton, N. S. Ponte, J. H. Whealton, and R. E. Wright, Rev. Sci. Instrum. 51, 1163 (1980).
13. C. C. Tsai, M. M. Menon, P. M. Ryan, D. E. Schechter, G. C. Barber, C. W. Blue, W. K. Dagenhart, R. R. Feezell, W. L. Gardner, H. H. Haselton, N. S. Ponte, W. L. Stirling, J. H. Whealton, and R. E. Wright, Bull. Am. Phys. Soc. 25(8), 971 (1980).
14. W. L. Stirling, H. H. Haselton, J. Kim, R. C. Davis, W. K. Dagenhart, W. L. Gardner, C. C. Tsai, J. H. Whealton, G. C. Barber, and R. E. Wright, Bull. Am. Phys. Soc. 23(7), 747 (1978).
15. J. Kim, W. L. Stirling, W. K. Dagenhart, G. C. Barber, H. H. Haselton, N. S. Ponte, C. C. Tsai, and R. E. Wright, 1979 IEEE International Conference on Plasma Science, 79CH1410-ONPS, p. 136.
16. W. L. Stirling, J. Kim, H. H. Haselton, G. C. Barber, R. C. Davis, W. K. Dagenhart, W. L. Gardner, N. S. Ponte, C. C. Tsai, J. H. Whealton, and R. E. Wright, Appl. Phys. Lett. 35(2), 104 (1979).

17. W. K. Dagenhart, P. M. Ryan, G. C. Barber, R. R. Feezell, W. L. Gardner, H. H. Haselton, M. M. Menon, N. S. Ponte, W. L. Stirling, C. C. Tsai, and J. H. Whealton, Bull. Am. Phys. Soc. 25(8), 983 (1980).

18. E. B. Hooper, Jr., and P. Poulsen, in Proc. 2nd Int. Symp. on the Production and Neutralization of Negative Hydrogen Ions and Beams, Brookhaven National Laboratory Report BNL-51304 (1980).

19. K. Prelec, in Proc. 2nd Int. Symp. on the Production and Neutralization of Negative Hydrogen Ions and Beams, Brookhaven National Laboratory Report BNL-51304 (1980).

20. W. K. Dagenhart, W. L. Stirling, H. H. Haselton, G. G. Kelley, J. Kim, C. C. Tsai, and J. H. Whealton, in Proc. 2nd Int. Symp. on the Production and Neutralization of Negative Hydrogen Ions and Beams, Brookhaven National Laboratory Report BNL-51304 (1980).

21. J. H. Fink and G. W. Hamilton, Lawrence Livermore National Laboratory Report UCID-18806 (1980).

22. M. Geoch, in Proc. 2nd Int. Symp. on the Production and Neutralization of Negative Hydrogen Ions and Beams, Brookhaven National Laboratory Report BNL-51304 (1980).

23. J. F. Clarke, G. G. Kelley, J. F. Lyon, and R. F. Stratton, in Plasma Physics and Controlled Nuclear Fusion Research (Proc. IAEA 3rd Conf., Novosibirsk, 1968), Vol. 2, IAEA, Vienna (1969).

24. C. Schmidt, in Proc. 2nd Int. Symp. on the Production and Neutralization of Negative Hydrogen Ions and Beams, Brookhaven National Laboratory Report BNL-51304 (1980).

25. L. O. Love, Science 182, 343 (1973).

26. J. R. Hiskes, A. Karo, and M. Gardner, J. Appl. Phys. 47, 3888 (1976); J. R. Hiskes and A. Karo, Lawrence Livermore National Laboratory Report UCRL-79512 (1977).

27. V. Buchanan, R. Clipperton, M. Grossman, W. Hensel, M. Kobayashi, R. Larson, E. McKenna, K. Prelec, T. Sluyters, and F. Usack, Brookhaven National Laboratory AGS Division H^- Technical Note #7, 1975.

28. Yu. I. Bel'chenko, G. I. Dimov, and V. G. Dudnikov, in Proc. Symp. on the Production and Neutralization of Negative Hydrogen Ion Beams, Brookhaven National Laboratory Report BNL-50727 (1977).

29. K. Prelec, in Proc. Symp. on the Production and Neutralization of Negative Hydrogen Ion Beams, Brookhaven National Laboratory Report BNL-50727 (1977).

30. P. W. Allison, in Proc. Symp. on the Production and Neutralization of Negative Hydrogen Ion Beams, Brookhaven National Laboratory Report BNL-50727 (1977).

31. W. K. Dagenhart and T. W. Whitehead, Jr., Nucl Instrum. Methods 85, 215 (1970).

32. A. Guthrie and R. K. Wakerling, *Electromagnetic Separation Project*, National Nuclear Energy Series, Division I, Vol. 5, McGraw-Hill, New York, 1949.

33. W. K. Dagenhart and W. L. Stirling, Electron Energy Recovery System for Negative Ion Sources, patent applied for September 1980, #187915.

34. R. K. Wakerling and A. Guthrie, *Electromagnetic Separation Project*, National Nuclear Energy Series, Division I, Vol. 4, McGraw-Hill, New York, 1951.

35. W. K. Dagenhart, W. L. Stirling, and C. C. Tsai, Bull. Am. Phys. Soc. 23(7), 805 (1978).

36. V. G. Dudnikov, Proc. 4th U.S.S.R. National Conf. on Particle Accelerators, p. 323 (Russian) (1975).

37. K. Prelec, Nucl. Instrum. Methods 144, 413 (1977).

38. J. R. Hiskes and A. Karo, in Proc. Symp. on the Production and Neutralization of Negative Hydrogen Ion Beams, Brookhaven National Laboratory Report BNL-50727 (1977).

39. Yu. I. Bel'chenko and V. G. Dudnikov, in Proc. 4th U.S.S.R. Conf. on Atomic Particle Interactions with Solid State (Kharkov, 1976), Part III (in Russian), p. 180.

40. C. D. Moak, H. E. Banta, J. N. Thurston, J. W. Johnson, and R. F. King, Rev. Sci. Instrum. 30, 694 (1959).

41. G. G. Kelley (private communication, 1978).

42. Yu. I. Bel'chenko, G. I. Dimov, and V. G. Dudnikov, in Proc. Symp. on the Production and Neutralization of Negative Hydrogen Ion Beams, Brookhaven National Laboratory Report BNL-50727 (1977).

43. W. K. Dagenhart and W. L. Stirling, 1979 IEEE International Conference on Plasma Science, 79CH1410-ONPS, p. 31.

44. K. Prelec, panel discussion of Proc. Symp. on the Production and Neutralization of Negative Hydrogen Ion Beams, Brookhaven National Laboratory Report BNL-50727 (1977).

45. K. W. Ehlers and K. N. Leung, in Proc. 2nd Int. Symp. on the Production and Neutralization of Negative Hydrogen Ions and Beams, Brookhaven National Laboratory BNL-51302 (1980).

46. C. C. Tsai, R. R. Feezell, H. H. Haselton, P. M. Ryan, D. E. Schechter, W. L. Stirling, and J. H. Whealton, in Proc. 2nd Int. Symp. on the Production and Neutralization of Negative Hydrogen Ions and Beams, Brookhaven National Laboratory Report BNL-51304 (1980).

47. W. K. Dagenhart and W. L. Stirling, Bull. Am. Phys. Soc. 24, 972 (1979).

48. W. K. Dagenhart, W. L. Gardner, H. H. Haselton, M. M. Menon, D. E. Schechter, W. L. Stirling, and C. C. Tsai, in Proc. 7th Symp. on Engineering Problems of Fusion Research, Vol. 1, 77CH1267-4-NPS, p. 533 (1977).

49. K. Wiesemann, in Proc. Symp. on the Production and Neutralization of Negative Hydrogen Ion Beams, Brookhaven National Laboratory Report BNL-50727 (1977).

ORNL/TM-7895
Dist. Category UC-20

INTERNAL DISTRIBUTION

1. G. C. Barber
2. W. A. Bell, Jr.
3. D. H. Crandall
4-8. W. K. Dagenhart
9. R. A. Dory
10. C. A. Foster
11. W. L. Gardner
12. G. G. Kelley
13. M. M. Menon
14. D. Metzler
15. O. B. Morgan
16. E. Newman
17. N. S. Ponte
18. J. Rome
19. M. W. Rosenthal
20-24. P. M. Ryan
25. M. Saltmarsh
26. D. E. Schechter
27. J. Sheffield
28. V. C. Srivastava
29-33. W. L. Stirling
34-38. C. C. Tsai
39. J. Tracy
40. J. H. Wilgen
41. R. E. Wright
42-43. Central Research Library
44-45. Laboratory Records Department
46. Laboratory Records, ORNL-RC
47. ORNL Document Reference Section
48. ORNL Patent Office
49. ORNL — Y-12 Technical Library
50. Fusion Energy Division Reports Office
51. Fusion Energy Division Library

EXTERNAL DISTRIBUTION

52. J. G. Alessi, 930 Brookhaven National Laboratory, Accelerator Department, Upton, NY 11973
53. P. Allison, Los Alamos National Laboratory, P.O. Box 1663, Los Alamos, NM 87545
54. M. Bacal, Ecole Polytechnique, Laboratoire de Physique des Milieux, Palaiseau Cedex, 91128, France
55. W. L. Barr, Lawrence Livermore National Laboratory, University of California, Livermore, CA 94720
56. J. W. Beal, General Atomic Company, P.O. Box 81608, San Diego, CA 92138
57. K. H. Berkner, Lawrence Berkeley Laboratory, University of California, Berkeley, CA 94720
58. R. B. Campbell, Lawrence Livermore National Laboratory, MS L-644, Livermore, CA 94550
59. A. Colleraine, General Atomic Company, P.O. Box 81608, San Diego, CA 92138
60. J. R. Conrad, University of Wisconsin, Department of Nuclear Engineering, Madison, WI 53706
61. D. H. Crandall, Oak Ridge National Laboratory, P.O. Box X, Oak Ridge, TN 37830
62. S. O. Dean, Science Applications, Inc., 2 Professional Drive, Suite 249, Gaithersburg, MD 20760

63. K. W. Ehlers, Lawrence Berkeley Laboratory, University of California, Berkeley, CA 94720
64. H. P. Eubank, Princeton Plasma Physics Laboratory, P.O. Box 451, Princeton, NJ 08544
65. J. W. Fink, L-434, Lawrence Livermore National Laboratory, P.O. Box 808, Livermore, CA 94550
66. A. T. Forrester, University of California, Physics Department, Los Angeles, CA 90024
67. R. Geller, Centre d'Etudes Nucleaires, Departmente de Physique du Plasma et de la Fusion Controlee, 85 X Grenoble, Cedex, France
68. W. G. Graham, New University of Ulster, Physics Department, Coleraine BT 52 1Sa, Northern Ireland
69. T. S. Green, Culham Laboratory, Abingdon, Oxfordshire, United Kingdom
70. G. W. Hamilton, Lawrence Livermore National Laboratory, P.O. Box 808, Livermore, CA 94550
71. D. Hinshelwood, Massachusetts Institute of Technology, 167 Albany Street, Room 36-297, Cambridge, MA 02139
72. J. R. Hiskes, Lawrence Livermore National Laboratory, P.O. Box 808, Livermore, CA 94550
73. A. J. Holmes, Culham Laboratory, Applied Physics & Technology Division, Abingdon, Oxfordshire, OX14 3DB, United Kingdom
74. R. Huse, Chairman, EPRI Fusion Program Committee, Public Service Electric and Gas Company, 80 Park Place, Newark, NJ 07101
75. J. Kim, General Atomic Company, P.O. Box 81608, San Diego, CA 92138
76. K. N. Leung, Lawrence Berkeley Laboratory, University of California, Berkeley, CA 94720
77. Library, Max Planck Institut fur Plasmaphysik, Garching bei Munchen, Federal Republic of Germany
78. Library, Princeton Plasma Physics Laboratory, P.O. Box 451, Princeton, NJ 08540
79. X. Z. Li, University of Wisconsin, Nuclear Engineering Department, 1500 Johnson Drive, Madison, WI 53706
80. J. Los, FOM-Institute for Atoma and Molecule Physics, Kruislaan 407, 1098 SJ Amsterdam, The Netherlands
81. S. Matsuda, Japan Atomic Energy Research Institute, Tokai, Ibaraki, Japan
82. R. W. Moir, Lawrence Livermore National Laboratory, University of California, P.O. Box 808, Livermore, CA 94551
83. T. Ohkawa, General Atomic Company, P.O. Box 81608, San Diego, CA 92138
84. M. Otsuka, JAERI Team, General Atomic Company, P.O. Box 81608, San Diego, CA 92138
85. K. Prelec, 911B Brookhaven National Laboratory, Accelerator Department, Upton, NY 11973
86. R. V. Pyle, Lawrence Berkeley Laboratory, University of California, Berkeley, CA 94720
87. G. Schilling, Princeton Plasma Physics Laboratory, P.O. Box 451, Princeton, NJ 08544
88. C. W. Schmidt, Fermi National Accelerator Laboratory, P.O. Box 500, Batavia, IL 60510

89. M. Seidl, Stevens Institute of Technology, Castle Point Station, Hoboken, NJ 07030
90. T. Sluyters, Brookhaven National Laboratory, Upton, Long Island, NY 11973
91. H. V. Smith, Los Alamos National Laboratory, P.O. Box 1663, Los Alamos, NJ 87545
92. E. Speth, Max Planck Institut fur Plasmaphysik, Garching bei Munchen, West Germany
93. H. S. Staten, Office of Fusion Energy, Department of Energy, Washington, DC 20545
94. L. D. Stewart, Princeton Plasma Physics Laboratory, P.O. Box 451, Princeton, NJ 08544
95. R. Stinnett, Division 4234, Sandia National Laboratory, Albuquerque, NM 87109
96. K. Takayama, Director, Institute of Plasma Physics, Nagoya University, Nagoya, Japan
97. E. Thompson, Culham Laboratory, Abingdon, Oxfordshire, United Kingdom
98. K. Yoshikaw, Institute of Atomic Energy, Kyoto University, Uzi, Kyoto, 611, Japan
99. Office of Assistant Manager for Energy Research and Development, Department of Energy, Oak Ridge Operations, P.O. Box E, Oak Ridge, TN 37830

100-221. Given distribution as shown in TID-4500, Magnetic Fusion Energy (Distribution Category UC-20)

☆U.S. GOVERNMENT PRINTING OFFICE: 1982-54